Article

Cell

Antibacterial Nucleoside-Analog Inhibitor of Bacterial RNA Polymerase

Graphical Abstract

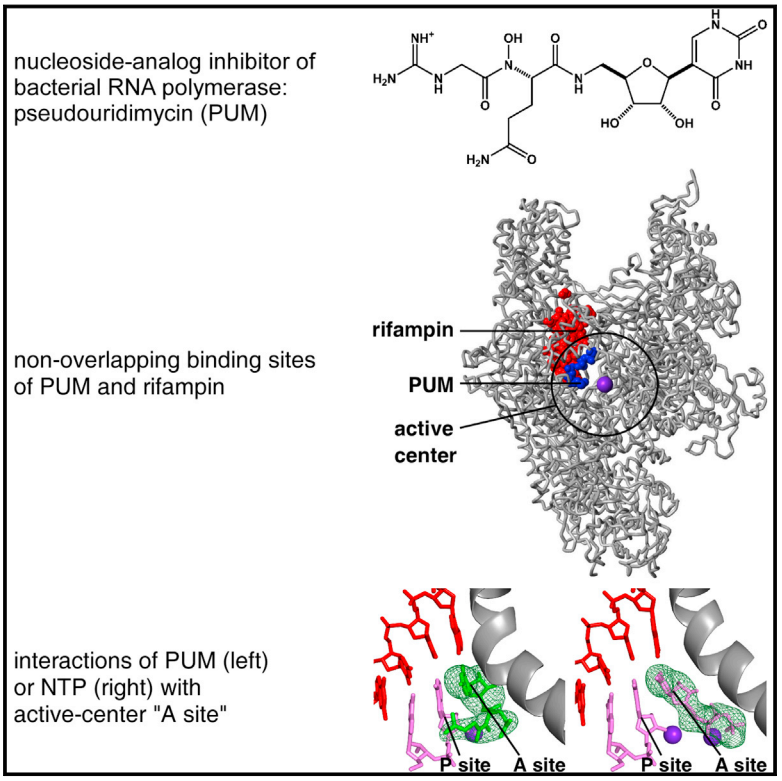

Authors

Sonia I. Maffioli, Yu Zhang, David Degen, ..., Gianni Dehò, Stefano Donadio, Richard H. Ebright

Correspondence

sdonadio@naicons.com (S.D.), ebright@waksman.rutgers.edu (R.H.E.)

In Brief

Pseudouridimycin competes with incoming nucleotides to inhibit bacterial RNA polymerase, effectively blocking growth of a broad range of pathogens.

Highlights

- New antibiotic from microbial extract screening
- Selective nucleoside-analog inhibitor of bacterial RNA polymerase
- Competition with UTP for occupancy of RNAP active-center NTP addition site
- Low resistance rate due to functional constraints on substitution of active center

Maffioli et al., 2017, Cell *169*, 1240–1248
June 15, 2017
http://dx.doi.org/10.1016/j.cell.2017.05.042

CellPress

Cell

Article

Antibacterial Nucleoside-Analog Inhibitor of Bacterial RNA Polymerase

Sonia I. Maffioli,[1,2,7] Yu Zhang,[3,7] David Degen,[3,7] Thomas Carzaniga,[4] Giancarlo Del Gatto,[1] Stefania Serina,[1,2] Paolo Monciardini,[1,2] Carlo Mazzetti,[1] Paola Guglierame,[5] Gianpaolo Candiani,[2] Alina Iulia Chiriac,[6] Giuseppe Facchetti,[2] Petra Kaltofen,[2] Hans-Georg Sahl,[6] Gianni Dehò,[4] Stefano Donadio,[1,2,*] and Richard H. Ebright[3,8,*]

[1]NAICONS Srl, 20139 Milan, Italy
[2]Vicuron Pharmaceuticals, 21040 Gerenzano, Italy
[3]Waksman Institute and Department of Chemistry, Rutgers University, Piscataway, NJ 08854, USA
[4]Department of Bioscience, University of Milan, 20122 Milan, Italy
[5]NeED Pharma Srl, 20139 Milan, Italy
[6]Institute of Medical Microbiology, Immunology, and Parasitology, University of Bonn, D-53012 Bonn, Germany
[7]Contributed equally
[8]Lead contact: ebright@waksman.rutgers.edu
*Correspondence: sdonadio@naicons.com (S.D.), ebright@waksman.rutgers.edu (R.H.E.)
http://dx.doi.org/10.1016/j.cell.2017.05.042

SUMMARY

Drug-resistant bacterial pathogens pose an urgent public-health crisis. Here, we report the discovery, from microbial-extract screening, of a nucleoside-analog inhibitor that inhibits bacterial RNA polymerase (RNAP) and exhibits antibacterial activity against drug-resistant bacterial pathogens: pseudouridimycin (PUM). PUM is a natural product comprising a formamidinylated, N-hydroxylated Gly-Gln dipeptide conjugated to 6′-amino-pseudouridine. PUM potently and selectively inhibits bacterial RNAP in vitro, inhibits bacterial growth in culture, and clears infection in a mouse model of *Streptococcus pyogenes* peritonitis. PUM inhibits RNAP through a binding site on RNAP (the NTP addition site) and mechanism (competition with UTP for occupancy of the NTP addition site) that differ from those of the RNAP inhibitor and current antibacterial drug rifampin (Rif). PUM exhibits additive antibacterial activity when co-administered with Rif, exhibits no cross-resistance with Rif, and exhibits a spontaneous resistance rate an order-of-magnitude lower than that of Rif. PUM is a highly promising lead for antibacterial therapy.

INTRODUCTION

There is an urgent need for new antibacterial drugs effective against bacterial pathogens resistant to current drugs (reviewed in Marston et al., 2016; Brown and Wright, 2016).

Bacterial RNA polymerase (RNAP) is a proven target for broad-spectrum antibacterial therapy (reviewed in Mariani and Maffioli, 2009; Ho et al., 2009; Aristoff et al., 2010; Srivastava et al., 2011). The suitability of bacterial RNAP as a target for broad-spectrum antibacterial therapy follows from the fact that bacterial RNAP is an essential enzyme (permitting efficacy), the fact that bacterial RNAP subunit sequences are highly conserved (providing a basis for broad-spectrum activity), and the fact that bacterial RNAP-subunit sequences are not highly conserved in eukaryotic RNAP I, RNAP II, and RNAP III (providing a basis for therapeutic selectivity).

RNAP is the target of two classes of antibacterial drugs currently in clinical use: (1) rifamycins (rifampin [Rif], rifapentine, rifabutin, and rifamixin), which function by binding to a site adjacent to the RNAP active center and sterically inhibiting extension of short RNA products (Campbell et al., 2001; Feklistov et al., 2008; Lin et al., 2017); and (2) lipiarmycins (fidaxomicin), which function by binding to a site distant from the RNAP active center and allosterically inhibiting initial RNAP-DNA interaction (Ebright, 2005; Srivastava et al., 2011). Bacterial RNAP also is the target of a class of antibacterial agents currently in preclinical development: myxopyronins, which function by binding to a site distant from the RNAP active center and allosterically inhibiting opening of, and loading of DNA into, the RNAP active-center cleft (Mukhopadhyay et al., 2008; Belogurov et al., 2009; Srivastava et al., 2011). Rifamycins, lipiarmycins, and myxopyronins are subject to spontaneous resistance emergence (Mariani and Maffioli, 2009; Ho et al., 2009; Aristoff et al., 2010; Srivastava et al., 2011, 2012). Resistance to rifamycins, lipiarmycins, and myxopyronins arises from mutations that result in substitution of the respective binding sites on RNAP for the compounds, preventing binding of the compounds.

Nucleoside-analog inhibitors (NAIs) that selectively inhibit viral nucleotide polymerases have had transformative impact on treatment of HIV (e.g., AZT, DDI, DDC, 3TC, d4T, and tenofovir; reviewed in Cihlar and Ray, 2010) and HCV (e.g., sofosbuvir; reviewed in Summers et al., 2014). NAIs that selectively inhibit bacterial RNAP potentially could have an analogous impact on the treatment of bacterial infections, particularly because functional constraints on substitution of RNAP nucleoside-triphosphate (NTP) binding sites could limit substitutions that confer resistance (Summers et al., 2014; Zhang et al., 2014).

Here, we report the discovery, from microbial-extract screening, of the first NAI that selectively inhibits bacterial RNAP.

A

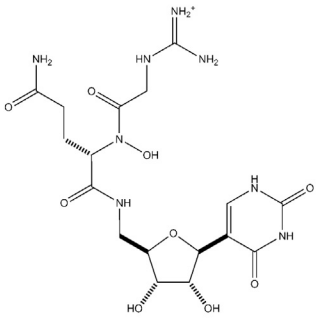

B RNAP-inhibitory activity of PUM

RNAP	IC50 (μM)
Gram-positive bacterial RNAP	
Staphylococcus aureus RNAP	0.1
Rif-resistant *Bacillus subtilis* RNAP [469 (513) Gln→Arg]β-RNAP	0.1
Gram-negative bacterial RNAP	
Escherichia coli RNAP	0.1
Rif-resistant *Escherichia coli* RNAP (531 Ser→Leu)β-RNAP	0.1
Human RNAP	
Human RNAP I	>50
Human RNAP II	1
Human RNAP III	9
Viral RNAP	
SP6 RNAP	>50
T7 RNAP	>50
Φ6 RNAP (RNA-dependent RNAP)	>50

C

antibacterial activity of PUM *in vitro*

organism	IC50 (μM)
Gram-positive bacteria	
Streptococcus pyogenes L49	4
Streptococcus pyogenes L49 in the presence of 30% human serum	4
Streptococcus pneumoniae L44	4
Streptococcus pneumoniae L44 in the presence of 30% human serum	4
Streptococcus pneumoniae L899 (Rif-resistant)	6
Streptococcus pneumoniae L1407 (Azi-resistant)	6
Streptococcus pneumoniae ND061311 (Pen-Azi-resistant)	6
Streptococcus pneumoniae L3909 (Pen-Ery-Chl-Ctr-resistant)	4
Streptococcus pneumoniae L1542 (Ery-Cli-Ami-Gen-Tet-resistant)	6
Streptococcus pneumoniae L2868 (Met-Oxa-Ery-Cli-Ami-Gen-Tet-Tri-Chl-resistant)	6
Staphylococcus aureus ATCC 12600	8
Staphylococcus aureus ATCC 12600-S531L (Rif-resistant)	8
Staphylococcus aureus BAA-1707 (Met-resistant)	4
Staphylococcus aureus CB1616 (Met-Dap-resistant)	8
Staphylococcus aureus NRS120 (Met-Cip-Gen-Tet-Tri-Lin-resistant)	16
Staphylococcus aureus NRS1 (Rif-Met-Cip-Ery-Cli-Gen-Tet-Dap-resistant; Van-intermediate)	16
Staphylococcus aureus VRS1 (Rif-Met-Cip-Ery-Cli-Gen-Mup-Tec-Van-resistant)	8
Enterococcus faecium ATCC 19434	4
Gram-negative bacteria	
Haemophilus influenzae L3296	2
Moraxella catarrhalis L3294	2
Human cells	
Human macrovascular endothelial	>100
Human monocyte	>100

D

antibacterial activity of PUM *in vivo*: mouse *Streptococcus pyogenes* peritonitis model

organism	ED50 (total dose; mg/kg) (95% confidence interval)
intravenous (iv) administration, 10 min and 6 h post-infection	9 (5-20)
intravenous (iv) administration, 10 min post-infection	20 (3-100)
subcutaneous (sc) administration, 10 min post-infection	30 (20-40)

E

absence of cross-resistance between PUM and Rif

amino acid substitution	resistance level ($MIC/MIC_{wild\text{-}type}$)	
	Rif	PUM
***rpoB* (RNAP β subunit)**		
135 (146) Val→Phe	>2048	1
472 (512) Ser→Pro	64	1
473 (513) Gln→Arg	>2048	1
473 (513) Gln→Lys	>2048	1
476 (516) Asp→Asn	32	1
476 (516) Asp→Tyr	256	1
476 (516) Asp→Val	>2048	1
482 (522) Ser→Leu	>2048	1
486 (526) His→Tyr	>2048	1
491 (531) Ser→Phe	>2048	1
491 (531) Ser→Tyr	>2048	1
494 (534) Gly→Val	128	0.5
524 (564) Pro→Leu	512	4

F

additive antibacterial activity of PUM and Rif

organism	$FICI_{min}$	$FICI_{max}$	interaction type
Streptococcus pyogenes L49	1.0	1.5	additive
Streptococcus pneumoniae L44	1.0	1.6	additive

Figure 1. Structure, RNAP-Inhibitory Activity, and Antibacterial Activity of PUM

(A) Structure of PUM.

(B) RNAP-inhibitory activity of PUM.

(C) Antibacterial activity of PUM in vitro. Drug resistances are as follows: Ami, amikacin; Azi, azithromycin; Cip, ciprofloxacin; Ctr, ceftriaxone; Dap, daptomycin; Ery, erythromycin; Chl, chloramphenicol; Cli, clindamycin; Gen, gentamicin; Lin, linezolid; Met, methicillin; Mup, mupirocin; Pen, penicillin; Ox, oxacillin; Rif, rifampin; Tec, teicoplanin; Tet, tetracycline; Tri, trimethoprim; Van, vancomycin.

(D) Antibacterial activity of PUM in vivo.

(E) Absence of cross-resistance between PUM and Rif (data for *S. pyogenes* Rif-resistant mutants; residues numbered as in *S. pyogenes* and, in parentheses, *E. coli*).

(F) Additive antibacterial activity of PUM and Rif.

See Tables S1 and S2 and Figures S1 and S2.

RESULTS AND DISCUSSION

Identification of PUM

We screened a library of 3,000 Actinobacterial (Landwehr et al., 2016) and fungal culture extracts for the ability to inhibit RNAP, and we identified two extracts that inhibited bacterial RNAP (*E. coli* RNAP) but did not inhibit a structurally unrelated bacteriophage RNAP (SP6 RNAP) and did not contain a previously characterized inhibitor of bacterial RNAP (see Method Details). Fractionation of the two extracts by reversed-phase chromatography and structure elucidation of active components by mass spectrometry and multidimensional NMR spectrometry revealed that the extracts contained the same active component: pseudouridimycin (PUM; Figures 1A and S1).

RNAP-Inhibitory and Antibacterial Activity of PUM

PUM selectively inhibits bacterial RNAP (IC_{50} = 0.1 μM; selectivity >4- to >500-fold; Figures 1B and S2; Table S1), selectively

A

S. pyogenes spontaneous resistance rates

inhibitor	concentration	resistance rate (per generation) (95% confidence interval)
PUM	8x MIC	0.4×10^{-9} ($0.06\text{-}0.9 \times 10^{-9}$)
	16x MIC	0.5×10^{-9} ($0.1\text{-}1 \times 10^{-9}$)
Rif	8x MIC	3×10^{-9} ($1\text{-}6 \times 10^{-9}$)
	16x MIC	4×10^{-9} ($1\text{-}7 \times 10^{-9}$)

B

S. pyogenes PUM-resistant mutants: sequences and properties

amino acid substitution	number of isolates	resistance level ($MIC/MIC_{wild\text{-}type}$)
rpoB **(RNAP β subunit)**		
525 (565) Glu→Gly	1	>128
525 (565) Glu→Val	2	>128
643 (681) Met→Lys	2	>128
646 (684) Asn→Ile	1	16
rpoC **(RNAP β′ subunit)**		
791 (786) Thr→Arg	1	128
791 (786) Thr→Lys	2	>128
791 (786) Thr→Met	3	16

C

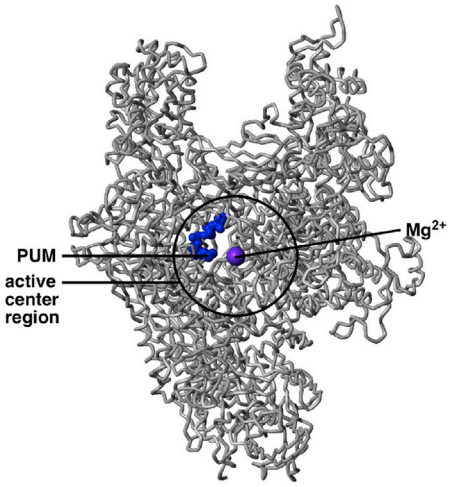

D

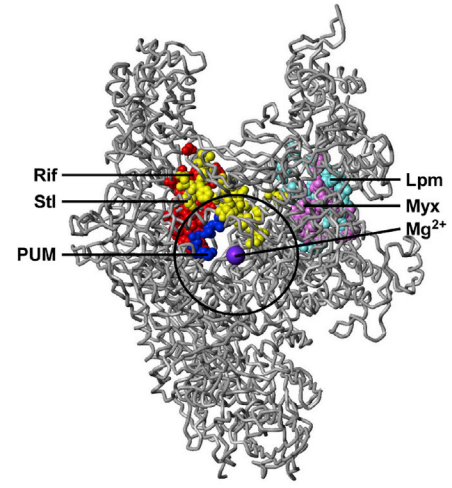

E

S. pyogenes PUM-resistant mutants: absence of high-level cross-resistance to Rif, Lpm, Myx, and Stl

amino acid substitution	resistance level ($MIC/MIC_{wild\text{-}type}$)			
	Rif	Lpm	Myx	Stl
rpoB **(RNAP β subunit)**				
525 (565) Glu→Gly	1	0.5	1	1
525 (565) Glu→Val	2	0.5	1	1
643 (681) Met→Lys	1	1	1	1
646 (684) Asn→Ile	16	1	1	0.5
rpoC **(RNAP β′ subunit)**				
791 (786) Thr→Arg	4	1	1	1
791 (786) Thr→Lys	1	1	1	1
791 (786) Thr→Met	1	1	1	1

Figure 2. Target of PUM: RNAP NTP Addition Site

(A) Spontaneous resistance rates for PUM and Rif.

(B) *S. pyogenes* spontaneous PUM-resistant mutants.

(C) Location of PUM target (blue) in three-dimensional structure of bacterial RNAP (Mukhopadhyay et al., 2008; gray; black circle for active-center region; violet sphere for active-center Mg^{2+}(I); β′ non-conserved region and σ omitted for clarity).

(D) Absence of overlap between PUM target (blue) and Rif (red), Lpm (cyan), Myx (pink), and Stl (yellow) targets.

(E), Absence of high-level cross-resistance for *S. pyogenes* PUM-resistant mutants to Rif, Lpm, Myx, and Stl.

See Figure S3.

inhibits bacterial growth (IC_{50} = 2–16 μM; selectivity >6- to >60-fold; Figure 1C), and clears infection in vivo in a mouse *Streptococcus pyogenes* peritonitis model (ED_{50} = 9 mg/kg; Figure 1C; Table S2). PUM exhibits antibacterial activity against both Gram-positive and Gram-negative bacteria and against both drug-sensitive and drug-resistant bacterial strains, including rifamycin-, β-lactam-, fluoroquinolone-, macrolide-, tetracycline-, aminoglycoside-, lincosamide-, chloramphenicol-, oxazolidinone-, trimethoprim-, glycopeptide-, lipopeptide-, mupirocin-, and multi-drug-resistant strains (Figure 1C).

PUM exhibits no cross-resistance with the classic RNAP inhibitor Rif (Figures 1B, 1C, and 1E), exhibits additive antibacterial activity when co-administered with Rif (Figure 1F), and exhibits spontaneous resistance rates an order-of-magnitude lower than those of Rif (Figure 2A), suggesting that PUM inhibits RNAP through a binding site and mechanism different from those of Rif.

Target of Transcription Inhibition by PUM

Gene sequencing indicates that PUM-resistant mutants contain mutations in the *rpoB* gene (encodes RNAP β subunit) or the *rpoC* gene (encodes RNAP β′ subunit), confirming that RNAP is the functional cellular target of PUM (Figures 2B, S3A, and S3B). In the Gram-positive bacterium *S. pyogenes*, substitutions conferring ≥4x PUM resistance are obtained at four sites: β residues 565, 681, and 684 and β′ residue 786 (numbered as in *E. coli* RNAP; Figure 2B). In the Gram-negative bacterium *E. coli*, substitutions conferring PUM resistance are obtained at two sites: β residues 565 and 681 (Figures S3A and S3B). The number of sites of substitutions conferring PUM resistance is an order-of-magnitude lower than the number of sites of substitutions conferring Rif-resistance (2–4 versus 25; Jin and Gross, 1988; Garibyan et al., 2003), consistent with, and accounting for, the observation that spontaneous resistance rates for PUM are an order-of-magnitude lower than those for Rif (Figure 2A).

Mapping the sites of substitutions conferring PUM resistance onto the three-dimensional structure of bacterial RNAP shows that the sites form a single discrete cluster (“PUM target”; Figures 2C and S3D). The PUM target is located within the RNAP active-center region and overlaps the RNAP active-center NTP addition site (“A site” also referred to as “i+1 site”; Figures 2C and S3D), suggesting that PUM inhibits RNAP by interfering with function of the NTP addition site. The PUM target is different from, and does not overlap, the Rif target (Figures 2D and S3E; Jin and Gross, 1988; Campbell et al., 2001; Garibyan et al., 2003), consistent with, and accounting for, the observation that PUM does not

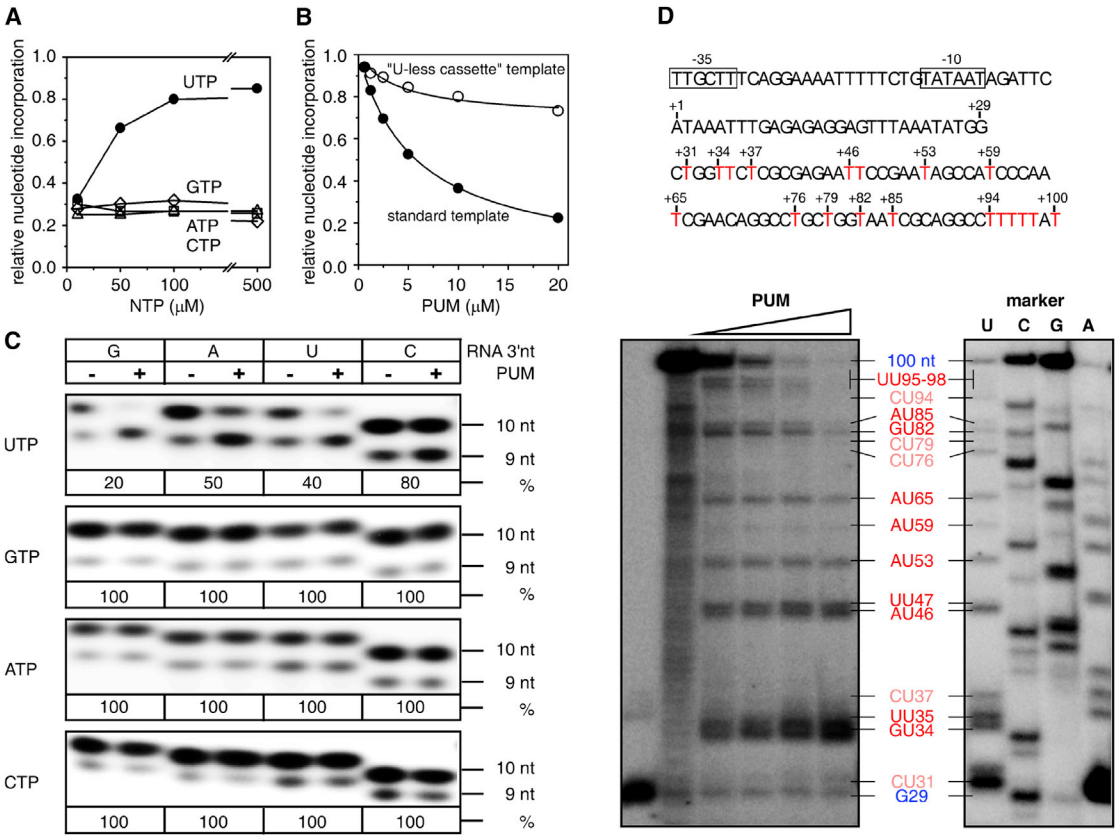

Figure 3. Mechanism of PUM: Competition with UTP for Occupancy of RNAP NTP Addition Site

(A) Suppression of inhibition by PUM by high [UTP], but not high [GTP], [ATP], or [CTP] (*E. coli* RNAP).

(B) Inhibition by PUM of transcription directing incorporation of U+G+A+C, but not "U-less" transcription directing incorporation of G+A+C (*E. coli* RNAP).

(C) Single-nucleotide-addition reactions showing that inhibition by PUM requires template positions directing incorporation of U (row 1) and prefers preceding template positions directing incorporation of G, A, or U (columns 1–3) (*E. coli* RNAP; 2.5 μM NTPs). UTP, GTP, ATP, or CTP (left), incoming NTP; G, A, U, or C (top), nucleotide at RNA 3′ end; 9 nt RNA (right), precursor for single-nucleotide addition; 10 nt RNA (right), product of single-nucleotide addition; % (right), percent yield of 10 nt RNA in presence of PUM versus in absence of PUM.

(D) Multiple-nucleotide-addition reactions showing that inhibition by PUM requires template positions directing incorporation of U (red GU, AU, or UU, and pink CU) and prefers preceding template positions directing incorporation of G, A, or U (red GU, AU, or UU) (*E. coli* RNAP; 10 μM NTPs).See Figure S4.

share cross-resistance with Rif (Figures 1B, 1C, 1E, 2E, S3F, and S3G) and the observation that PUM and Rif exhibit additive antibacterial activity (Figure 1F). The PUM target also is different from, and does not overlap, the targets of the RNAP inhibitors lipiarmycin (Lpm) (Ebright, 2005; Srivastava et al., 2011), myxopyronin (Myx) (Mukhopadhyay et al., 2008; Belogurov et al., 2009; Srivastava et al., 2011), streptolydigin (Stl) (Tuske et al., 2005; Temiakov et al., 2005), CBR703 (CBR) (Feng et al., 2015; Bae et al., 2015), and salinamide (Sal) (Degen et al., 2014; Figures 2D and S3E), and, correspondingly, PUM does not exhibit cross-resistance with Lpm, Myx, Stl, CBR703, and Sal (Figures 2E, S3F, S3H, and S3I). The PUM target partly overlaps the target for the RNAP inhibitor GE23077 (GE) (Figure S3M; Zhang et al., 2014), and, correspondingly, PUM exhibits partial cross-resistance with GE (Figure S3N).

Biochemical Basis of Transcription Inhibition by PUM

The observation that PUM is an NAI that has the same Watson-Crick base-pairing specificity as UTP (Figure 1A) and the observation that the PUM target overlaps the RNAP NTP addition site (Figures 2B and S3A) suggest the hypothesis that PUM functions as an NAI that competes with UTP for occupancy of the RNAP NTP addition site. Five biochemical results support this hypothesis. First, PUM inhibits transcription by inhibiting nucleotide addition (Figure S4). Second, high concentrations of UTP—but not high concentrations of GTP, ATP, or CTP—overcome transcription inhibition by PUM (Figure 3A). Third, PUM inhibits transcription only on templates that direct incorporation of U (Figure 3B). Fourth, in single-nucleotide-addition transcription reactions, PUM inhibits incorporation of U, but not G, A, or C (Figure 3C). Fifth, in multiple-nucleotide-addition transcription reactions, PUM inhibits incorporation of U, but not G, A, or C (Figure 3D). The results in Figures 3C and 3D further establish that transcription inhibition by PUM not only requires a template position that directs incorporation of U but also strongly prefers a preceding template position that directs incorporation of G, A, or U. We conclude that PUM functions as an NAI that competes with UTP at positions

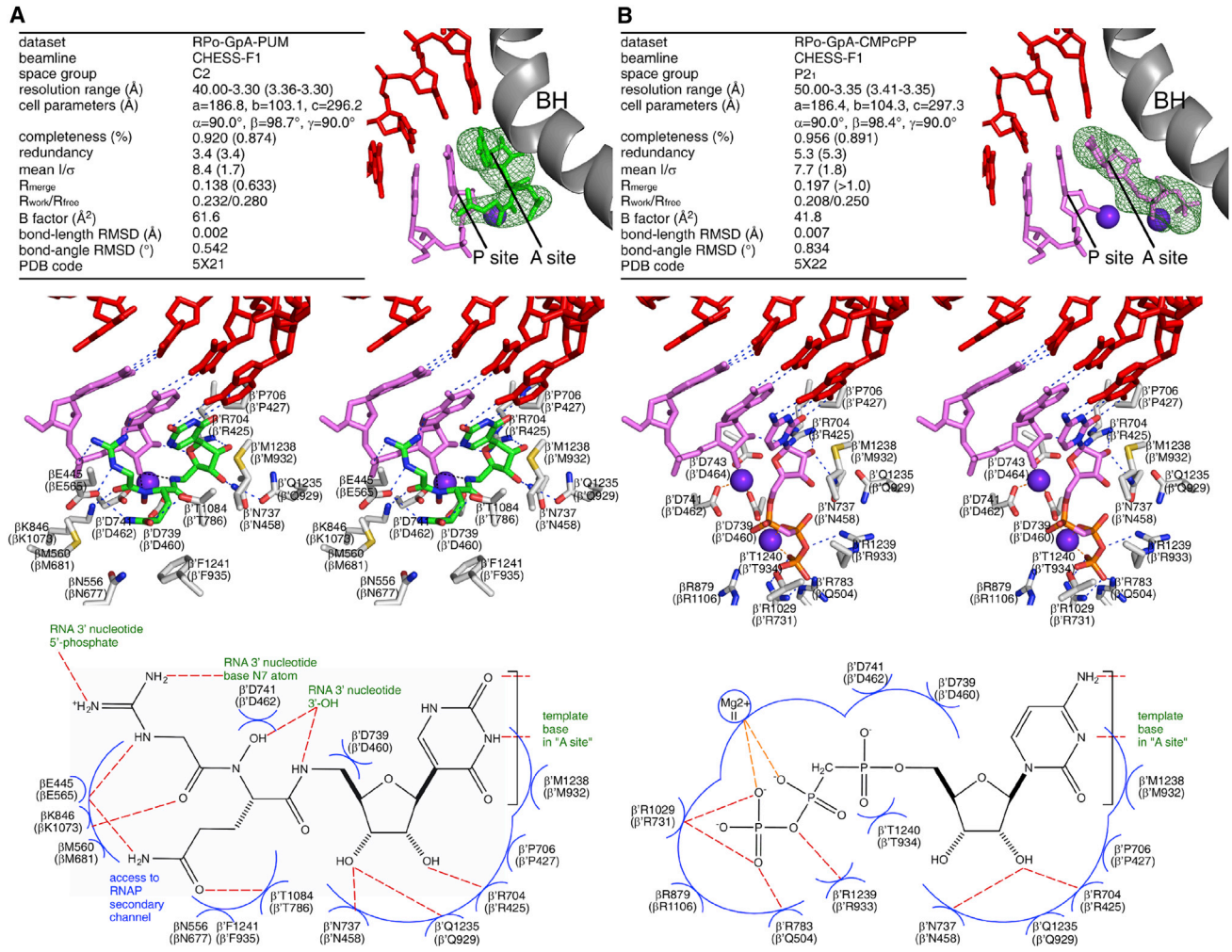

Figure 4. Structural Basis of Transcription Inhibition by PUM

(A and B) Structures of *T. thermophilus* transcription initiation complexes containing PUM (A) and CMPcPP (B). Top: Crystallization and refinement statistics (left) and experimental electron density and fit (right). Green, PUM; pink, RNA and CMPcPP; red, DNA template strand; violet sphere between RNAP product (P) and addition (A) sites, Mg^{2+}(I); violet sphere in RNAP addition (A) site, Mg^{2+}(II); gray, RNAP bridge helix; green mesh, mF_o-DF_c omit map (contoured at 2.5 σ). Middle: Stereodiagram of interactions. Green, PUM carbon atoms; pink, RNA and CMPcPP carbon atoms; gray, RNAP carbon atoms; red, blue, yellow, and orange, oxygen, nitrogen, sulfur, and phosphorous atoms; dashed lines, H bonds; other colors, as above. Bottom: Summary of interactions. Red dashed lines, H bonds; blue arcs, Van der Waals interactions. Residues numbered as in *T. thermophilus* RNAP and, in parentheses, *E. coli* RNAP.
See Table S3 and Figure S5.

that direct incorporation of U preceded by positions that direct incorporation of G, A, or U.

Structural Basis of Transcription Inhibition by PUM

To define the structural basis of transcription inhibition by PUM, we determined a crystal structure of a transcription initiation complex containing PUM (RPo-GpA-PUM; Figure 4A) and, for comparison, a crystal structure of a corresponding transcription initiation complex containing CMPcPP, a non-hydrolysable NTP analog shown previously to be able to stably occupy the RNAP NTP addition site (Zhang et al., 2014) (RPo-GpA-CMPcPP; Figure 4B). The results establish that PUM is an NAI that competes for occupancy of the RNAP NTP addition site (Figure 4). PUM binds to the NTP addition site (Figure 4A). The PUM base makes Watson-Crick hydrogen bonds with a DNA template-strand A in a manner equivalent to an NTP base; the PUM sugar moiety makes interactions with the NTP addition site in a manner nearly equivalent to an NTP sugar; the PUM glutamine moiety makes interactions that mimic interactions made by an NTP triphosphate; and the PUM N-hydroxy and guanidinyl moieties interact with the RNA nucleotide base-paired to the preceding template position (RNA 3′ nucleotide), with the N-hydroxy donating a hydrogen bond to the 3′ OH of the RNA 3′ nucleotide and the guanidinyl moiety donating one hydrogen bond to the 5′ phosphate of the RNA 3′ nucleotide and another to the base of the RNA 3′ nucleotide (Figure 4A).

The structure of the PUM-inhibited complex accounts for the observed specificity of inhibition for template positions that

A

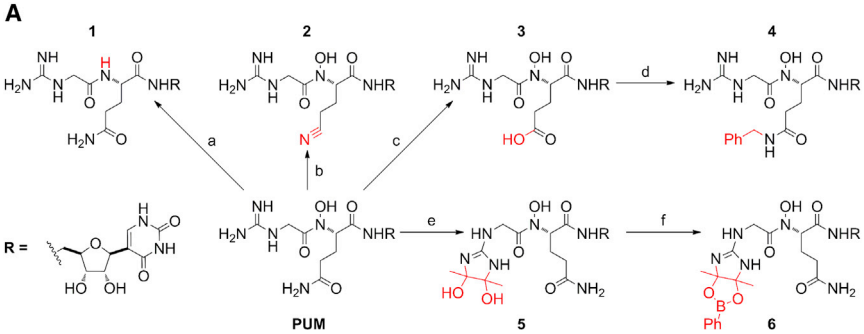

(a) $TiCl_3$, 1M NaOAc (pH 7), RT 2h, 100%; (b) $PdCl_2$, 1:1 ACN:H_2O, RT 2h, 90%; (c) 0.1% TFA, RT 3 days, 100%; (d) $BnNH_2$, DMF + PyBOP, RT 30min, 100%; (e) 2,3-butanedione, 10mM NH_4OAc (pH 8), RT 30min, 100%; (f) $PhB(OH)_2$, 10 mM NH_4OAc (pH 8), RT 2h, 100%

B

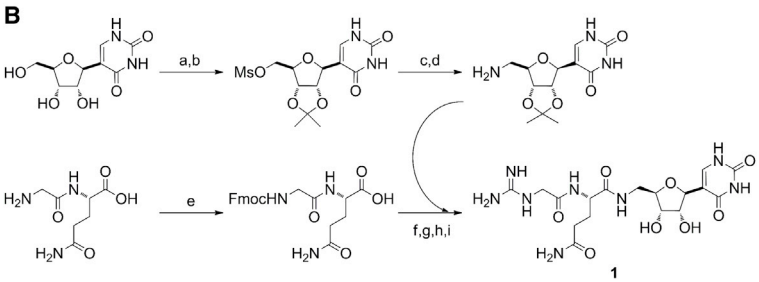

(a) $Me_2C(OMe)_2$, DMF, HCl, RT 5h, 100%; (b) MsCl, Pyr, 0°C + RT 16h, 95%; (c) NaN_3, DMF, 100°C 4h, 86%; (d) Me_3P, THF + H_2O, RT 2h, 95%; (e) Na_2CO_3 + FmocCl, dioxane + H_2O, RT o/n, 100%; (f) DCC-HOBT, dry DMF, RT o/n, 95%; (g) piperidine, DMF, 25°C 10min, 100%; (h) 3,5-dimethylpyrazole-1-carboxyamidine, MeOH, RT o/n + 65°C 6h, 100%; (i) 7:3 AcOH-H_2O, RT o/n + 50°C 10h under Ar, 100%

C

RNAP-inhibitory activity (*E. coli* RNAP)

PUM derivative	IC50 (μM)
PUM	0.3
1	4
2	>50
3	4
4	1
5	>50
6	>50

D

antibacterial activity (*S. pyogenes*)

PUM derivative	MIC (μg/ml)
PUM	2
1	16
2	>64
3	16
4	16
5	>64
6	>64

Figure 5. Semi-synthesis, Synthesis, and Analysis of PUM Derivatives

(A) Semi-synthesis of PUM derivatives lacking PUM N-hydroxy group (1), having alterations of PUM glutamine sidechain (2–4), or having alterations of PUM guanidinyl sidechain (5–6).

(B) Synthesis of PUM derivative lacking PUM N-hydroxy group (1).

(C and D) RNAP inhibitory activities and antibacterial activities of PUM derivatives.

direct incorporation of U preceded by template positions that direct incorporation of G, A, or U. The Watson-Crick base pair by the PUM base moiety with the DNA template strand provides absolute specificity for a position directing incorporation of U (Figure 4A). The hydrogen bond donated by the PUM guanidinyl moiety with the base of the RNA 3′ nucleotide confers specificity for a preceding position directing incorporation of G, A, or U (each of which contains a hydrogen-bond acceptor at the appropriate position; Figure 4A).

The structure also explains the selectivity of transcription inhibition by PUM. All RNAP residues contacted by PUM are highly conserved across Gram-positive and Gram-negative bacterial RNAP (Figure S5), accounting for the inhibition of both Gram-positive and Gram-negative bacterial RNAP. In contrast, four RNAP residues important for PUM are not conserved in human RNAP I, II, and III (β residues 677, 681, and 684 and β′ residue 932; Figure S5), accounting for selectivity for bacterial RNAP over human RNAP I, II, and III.

The structure also explains the small size of the PUM-resistance spectrum (four residues in *S. pyogenes* RNAP; two residues in *E. coli* RNAP; Figures 2B, S3A, and S3B). PUM makes direct contacts with RNAP residues at which PUM-resistant substitutions are obtained (Figure S5). However, PUM also makes direct contacts with ten other RNAP residues that comprise functionally critical residues of the RNAP active center that cannot be readily substituted without compromising RNAP activity (Sagitov et al., 1993; Svetlov et al., 2004; Sosunov et al., 2005; Jovanovic et al., 2011; Yuzenkova et al., 2012; Zhang et al., 2014) and thus that cannot be readily substituted to yield viable, fully fit, resistant mutants (Figure 4A; Zhang et al., 2014). We infer that PUM interacts with a "privileged target" for which most residues (10–12 of 14 residues) have functional constraints that limit substitution to yield viable resistant mutants. Similar results have been reported for the RNAP inhibitor GE, a non-nucleoside-analog inhibitor that binds to the RNAP active center (Zhang et al., 2014) and that exhibits a small target-based resistance spectrum (Zhang et al., 2014) (but that, unlike PUM, exhibits high non-target-based resistance, presumably at the level of uptake or efflux, precluding development as an antibacterial drug).

The structure enables structure-based design of PUM analogs with increased potency and increased selectivity. Initial lead-optimization efforts corroborate the importance of the PUM N-hydroxy, glutamine, and guanidinyl moieties and demonstrate that the PUM glutamine $C(O)NH_2$ can be replaced by C(O)NHR while retaining RNAP inhibitory and antibacterial activity (Figure 5).

Prospect

Our results provide a new class of antibiotic with activity against Gram-positive and Gram-negative bacteria in vitro and in vivo, no cross-resistance with current antibacterial

drugs, and low rates of resistance emergence. Our discovery of this class of antibiotic from conventional microbial extract screening indicates that, contrary to widespread belief (Marston et al., 2016), conventional microbial extract screening has not been exhausted as a source of antibacterial lead compounds.

Our results provide a selective NAI of bacterial RNAP. NAIs of viral nucleotide polymerases have been of immense importance for development of anti-HIV (Cihlar and Ray, 2010) and anti-HCV (Summers et al., 2014) drugs. NAIs of bacterial RNAP may show comparable promise for development of antibacterial drugs.

STAR★METHODS

Detailed methods are provided in the online version of this paper and include the following:

- KEY RESOURCES TABLE
- CONTACT FOR REAGENT AND RESOURCE SHARING
- EXPERIMENTAL MODEL AND SUBJECT DETAILS
  - Mice
  - Cell line and cell culture
- METHOD DETAILS
  - *E. coli* RNAP core enzyme
  - *E. coli* RNAP σ^{70} holoenzyme
  - *S. aureus* RNAP σ^{A} holoenzyme
  - *B. subtilis* RNAP σ^{A} holoenzyme
  - *T. thermophilus* RNAP σ^{A} holoenzyme
  - Microbial extract screening
  - Characterization of producer strains
  - Isolation and purification of pseudouridimycin
  - Structure elucidation of PUM
  - Effects of PUM on macromolecular synthesis
  - RNAP-inhibitory activity in vitro
  - Antibacterial activity in vitro
  - Antibacterial activity in vivo
  - Checkerboard interaction assays
  - Spontaneous resistance rate assays
  - Spontaneous PUM-resistant mutants, *S. pyogenes*
  - Spontaneous PUM-resistant mutants, *E. coli*
  - Resistance and cross-resistance levels
  - Formation of RNAP-promoter open complex
  - Nucleotide addition in transcription initiation
  - Nucleotide addition in transcription elongation
  - Nucleotide addition at elevated NTP concentrations
  - Nucleotide addition on standard and "U-less cassette" templates
  - Template-sequence specificity of inhibition by PUM: single-nucleotide-addition reactions
  - Template-sequence specificity of inhibition by PUM: multiple-nucleotide-addition reactions
  - Structure determination: RPo-GpA-PUM
  - Structure determination: RPo-GpA-CMPcPP
  - Semi-synthesis of PUM derivatives
  - Total synthesis of desoxy-PUM
- QUANTITATION AND STATISTICAL ANALYSIS
- DATA AVAILABILITY

SUPPLEMENTAL INFORMATION

Supplemental Information includes five figures and five tables and can be found with this article online at http://dx.doi.org/10.1016/j.cell.2017.05.042.

AUTHOR CONTRIBUTIONS

S.I.M. performed structure elucidation of PUM and semi-syntheses and syntheses of PUM derivatives. Y.Z. purified RNAP, assessed template-specificity of inhibition, and determined crystal structures. D.D. purified RNAP and assessed RNAP-inhibitory activities, antibacterial activities, resistance, and cross-resistance. T.C., S.S., and G.D. assessed RNAP-inhibitory activities. G.D.G. and C.M. purified PUM and participated in semi-syntheses and syntheses of PUM derivatives. P.M. performed characterization and fermentation of the PUM producer strain. P.G. and G.C. performed mouse infection studies. A.I.C. and H.-G.S. performed macromolecular synthesis assays. G.F. and P.K. performed microbial extract screening and de-replication. S.D. and R.H.E. designed the study, analyzed data, and wrote the paper.

ACKNOWLEDGMENTS

Work was supported by NIH grants GM041376 and AI104660 to R.H.E. and Italian Ministry of Research grant 30190679 and Regione Lombardia grants to NAICONS. We thank former colleagues at Vicuron Pharmaceuticals for early characterization of PUM; S. Parapini for cytotoxicity assays; W. Fenical for Sal; A. Berk and I. Grummt for plasmids; J. Silverman, NARSA, and BEI Resources for strains; and the Cornell High Energy Synchrotron Source for beamline access. S.I.M., S.S., P.M., and S.D. are employees and/or shareholders of NAICONS. Y.Z., S.I.M., S.S., P.M., P.G., G.C., S.D., and R.H.E. have patent filings. The other authors declare that no competing interests exist. (Vicuron Pharmaceuticals no longer is operational.)

Received: March 8, 2017
Revised: April 28, 2017
Accepted: May 26, 2017
Published: June 15, 2017

REFERENCES

Adams, P.D., Afonine, P.V., Bunkóczi, G., Chen, V.B., Davis, I.W., Echols, N., Headd, J.J., Hung, L.W., Kapral, G.J., Grosse-Kunstleve, R.W., et al. (2010). PHENIX: a comprehensive Python-based system for macromolecular structure solution. Acta Crystallogr. D Biol. Crystallogr. *66*, 213–221.

Aristoff, P.A., Garcia, G.A., Kirchhoff, P.D., and Showalter, H.D. (2010). Rifamycins–obstacles and opportunities. Tuberculosis (Edinb.) *90*, 94–118.

Bae, B., Nayak, D., Ray, A., Mustaev, A., Landick, R., and Darst, S.A. (2015). CBR antimicrobials inhibit RNA polymerase via at least two bridge-helix cap-mediated effects on nucleotide addition. Proc. Natl. Acad. Sci. USA *112*, E4178–E4187.

Barry, A.L., Pfaller, M.A., and Fuchs, P.C. (1993). Haemophilus test medium versus Mueller-Hinton broth with lysed horse blood for antimicrobial susceptibility testing of four bacterial species. Eur. J. Clin. Microbiol. Infect. Dis. *12*, 548–553.

Belogurov, G.A., Vassylyeva, M.N., Sevostyanova, A., Appleman, J.R., Xiang, A.X., Lira, R., Webber, S.E., Klyuyev, S., Nudler, E., Artsimovitch, I., and Vassylyev, D.G. (2009). Transcription inactivation through local refolding of the RNA polymerase structure. Nature *457*, 332–335.

Brown, E.D., and Wright, G.D. (2016). Antibacterial drug discovery in the resistance era. Nature *529*, 336–343.

Campbell, E.A., Korzheva, N., Mustaev, A., Murakami, K., Nair, S., Goldfarb, A., and Darst, S.A. (2001). Structural mechanism for rifampicin inhibition of bacterial RNA polymerase. Cell *104*, 901–912.

Ciciliato, I., Corti, E., Sarubbi, E., Stefanelli, S., Gastaldo, L., Montanini, N., Kurz, M., Losi, D., Marinelli, F., and Selva, E. (2004). Antibiotics GE23077,

novel inhibitors of bacterial RNA polymerase. I. Taxonomy, isolation and characterization. J. Antibiot. (Tokyo). *57*, 210–217.

Cihlar, T., and Ray, A.S. (2010). Nucleoside and nucleotide HIV reverse transcriptase inhibitors: 25 years after zidovudine. Antiviral Res. *85*, 39–58.

CLSI/NCCLS (Clinical and Laboratory Standards Institute) (2009). Methods for Dilution Antimicrobial Susceptibility Tests for Bacteria that Grow Aerobically; Approved Standard, Eighth Edition (Wayne, PA: CLIS Document), pp. M07–A8.

Dean, N., and Berk, A.J. (1988). Ordering promoter binding of class III transcription factors TFIIIC1 and TFIIIC2. Mol. Cell. Biol. *8*, 3017–3025.

Degen, D., Feng, Y., Zhang, Y., Ebright, K.Y., Ebright, Y.W., Gigliotti, M., Vahedian-Movahed, H., Mandal, S., Talaue, M., Connell, N., et al. (2014). Transcription inhibition by the depsipeptide antibiotic salinamide A. eLife *3*, e02451.

Donadio, S., Monciardini, P., and Sosio, M. (2009). Chapter 1. Approaches to discovering novel antibacterial and antifungal agents. Methods Enzymol. *458*, 3–28.

Ebright, R.H. (2005). RNA exit channel–target and method for inhibition of bacterial RNA polymerase. WIPO Patent Application WO/2005/001034, filed May 28, 2004, and published January 6, 2005.

Ebright, R.H., and Ebright, Y. (2012). Antibacterial agents: high-potency myxopyronin derivatives. WIPO Patent Application WO/2012037508, filed September 16, 2011, and published March 22, 2012.

Emsley, P., Lohkamp, B., Scott, W.G., and Cowtan, K. (2010). Features and development of Coot. Acta Crystallogr. D Biol. Crystallogr. *66*, 486–501.

Feklistov, A., Mekler, V., Jiang, Q., Westblade, L.F., Irschik, H., Jansen, R., Mustaev, A., Darst, S.A., and Ebright, R.H. (2008). Rifamycins do not function by allosteric modulation of binding of Mg2+ to the RNA polymerase active center. Proc Natl Acad Sci USA *105*, 14820–14825.

Feng, Y., Degen, D., Wang, X., Gigliotti, M., Liu, S., Zhang, Y., Das, D., Michalchuk, T., Ebright, Y.W., Talaue, M., et al. (2015). Structural basis of transcription inhibition by CBR hydroxamidines and CBR pyrazoles. Structure *23*, 1470–1481.

Fralick, J.A., and Burns-Keliher, L.L. (1994). Additive effect of *tolC* and *rfa* mutations on the hydrophobic barrier of the outer membrane of *Escherichia coli* K-12. J. Bacteriol. *176*, 6404–6406.

French, S., and Wilson, K. (1978). On the treatment of negative intensity observations. Acta Crystallogr. D Biol. Crystallogr. *34*, 517–525.

Friedman, L., Alder, J.D., and Silverman, J.A. (2006). Genetic changes that correlate with reduced susceptibility to daptomycin in *Staphylococcus aureus*. Antimicrob. Agents Chemother. *50*, 2137–2145.

Garibyan, L., Huang, T., Kim, M., Wolff, E., Nguyen, A., Nguyen, T., Diep, A., Hu, K., Iverson, A., Yang, H., and Miller, J.H. (2003). Use of the *rpoB* gene to determine the specificity of base substitution mutations on the *Escherichia coli* chromosome. DNA Repair (Amst.) *2*, 593–608.

Hall, B.M., Ma, C.X., Liang, P., and Singh, K.K. (2009). Fluctuation analysis CalculatOR: a web tool for the determination of mutation rate using Luria-Delbruck fluctuation analysis. Bioinformatics *25*, 1564–1565.

Hamilton, M., Russo, R., and Thurston, R. (1977). Trimmed Spearman-Karber method for estimating median lethal concentrations in toxicity bioassays. Environ. Sci. Technol. *11*, 714–719.

Hein, P.P., and Landick, R. (2010). The bridge helix coordinates movements of modules in RNA polymerase. BMC Biol. *8*, 141.

Ho, M.X., Hudson, B.P., Das, K., Arnold, E., and Ebright, R.H. (2009). Structures of RNA polymerase-antibiotic complexes. Curr Opin Structl Biol. *19*, 715–723.

Holowachuk, S.A., Bal'a, M.F., and Buddington, R.K. (2003). A kinetic microplate method for quantifying the antibacterial properties of biological fluids. J. Microbiol. Methods *55*, 441–446.

Hudson, B.P., Quispe, J., Lara-González, S., Kim, Y., Berman, H.M., Arnold, E., Ebright, R.H., and Lawson, C.L. (2009). Three-dimensional EM structure of an intact activator-dependent transcription initiation complex. Proc. Natl. Acad. Sci. USA *106*, 19830–19835.

Irschik, H., Gerth, K., Höfle, G., Kohl, W., and Reichenbach, H. (1983). The myxopyronins, new inhibitors of bacterial RNA synthesis from *Myxococcus fulvus* (Myxobacterales). J. Antibiot. (Tokyo). *36*, 1651–1658.

Irschik, H., Jansen, R., Höfle, G., Gerth, K., and Reichenbach, H. (1985). The corallopyronins, new inhibitors of bacterial RNA synthesis from Myxobacteria. J. Antibiot. (Tokyo). *38*, 145–152.

Irschik, H., Augustiniak, H., Gerth, K., Höfle, G., and Reichenbach, H. (1995). The ripostatins, novel inhibitors of eubacterial RNA polymerase isolated from myxobacteria. J. Antibiot. (Tokyo). *48*, 787–792.

Jin, D.J., and Gross, C.A. (1988). Mapping and sequencing of mutations in the *Escherichia coli rpoB* gene that lead to rifampicin resistance. J. Mol. Biol. *202*, 45–58.

Jokerst, R.S., Weeks, J.R., Zehring, W.A., and Greenleaf, A.L. (1989). Analysis of the gene encoding the largest subunit of RNA polymerase II in Drosophila. Mol. Gen. Genet. *215*, 266–275.

Jovanovic, M., Burrows, P.C., Bose, D., Cámara, B., Wiesler, S., Zhang, X., Wigneshweraraj, S., Weinzierl, R.O., and Buck, M. (2011). Activity map of the *Escherichia coli* RNA polymerase bridge helix. J. Biol. Chem. *286*, 14469–14479.

Kettenring, J., Colombo, L., Ferrari, P., Tavecchia, P., Nebuloni, M., Vékey, K., Gallo, G.G., and Selva, E. (1991). Antibiotic GE2270 a: a novel inhibitor of bacterial protein synthesis. II. Structure elucidation. J. Antibiot. (Tokyo). *44*, 702–715.

Lancini, G.C., and Sartori, G. (1968). Rifamycins LXI: in vivo inhibition of RNA synthesis of rifamycins. Experientia *24*, 1105–1106.

Lancini, G., Pallanza, R., and Silvestri, L.G. (1969). Relationships between bactericidal effect and inhibition of ribonucleic acid nucleotidyltransferase by rifampicin in *Escherichia coli* K-12. J. Bacteriol. *97*, 761–768.

Landwehr, W., Wolf, C., and Wink, J. (2016). Actinobacteria and Myxobacteria: two of the most important bacterial resources for novel antibiotics. Curr. Top. Microbiol. Immunol. *398*, 273–302.

Lane, W.J., and Darst, S.A. (2010). Molecular evolution of multisubunit RNA polymerases: sequence analysis. J. Mol. Biol. *395*, 671–685.

Leitner, A., and Lindner, W. (2003). Probing of arginine residues in peptides and proteins using selective tagging and electrospray ionization mass spectrometry. J. Mass Spectrom. *38*, 891–899.

Lin, W., Mandal, S., Degen, D., Liu, Y., Ebright, Y.W., Li, S., Feng, Y., Zhang, Y., Mandal, S., Jiang, Y., Liu, S., Gigliotti, M., Talaue, M., Connell, N., Das, K., Arnold, E., and Ebright, R.H. (2017). Structural basis of Mycobacterium tuberculosis transcription and transcription inhibition. Mol Cell. *66*, 169–179.

Ma, W., Sandri, G., and Sarkar, S. (1992). Analysis of the Luria-Delbrück distribution using discrete convolution powers. J. Appl. Probab. *29*, 255–267.

Maffioli, S.I., Marzorati, E., and Marazzi, A. (2005). Mild and reversible dehydration of primary amides with $PdCl_2$ in aqueous acetonitrile. Org. Lett. *7*, 5237–5239.

Mariani, R., and Maffioli, S.I. (2009). Bacterial RNA polymerase inhibitors: an organized overview of their structure, derivatives, biological activity and current clinical development status. Curr. Med. Chem. *16*, 430–454.

Marston, H.D., Dixon, D.M., Knisely, J.M., Palmore, T.N., and Fauci, A.S. (2016). Antimicrobial Resistance. JAMA *316*, 1193–1204.

Mattingly, P., and Miller, M. (1980). Titanium trichloride reduction of substituted N-hydroxy-2-azetidinones and other hydroxamic acids. J. Org. Chem. *45*, 410–415.

Mazza, P., Monciardini, P., Cavaletti, L., Sosio, M., and Donadio, S. (2003). Diversity of *Actinoplanes* and related genera isolated from an Italian soil. Microb. Ecol. *45*, 362–372.

Mazzetti, C., Ornaghi, M., Gaspari, E., Parapini, S., Maffioli, S., Sosio, M., and Donadio, S. (2012). Halogenated spirotetronates from *Actinoallomurus*. J. Nat. Prod. *75*, 1044–1050.

Meletiadis, J., Pournaras, S., Roilides, E., and Walsh, T.J. (2010). Defining fractional inhibitory concentration index cutoffs for additive interactions based on self-drug additive combinations, Monte Carlo simulation analysis, and

in vitro-in vivo correlation data for antifungal drug combinations against *Aspergillus fumigatus*. Antimicrob. Agents Chemother. *54*, 602–609.

Mukhopadhyay, J., Mekler, V., Kortkhonjia, E., Kapanidis, A.N., Ebright, Y.W., and Ebright, R.H. (2003). Fluorescence resonance energy transfer (FRET) in analysis of transcription-complex structure and function. Methods Enzymol. *371*, 144–159.

Mukhopadhyay, J., Das, K., Ismail, S., Koppstein, D., Jang, M., Hudson, B., Sarafianos, S., Tuske, S., Patel, J., Jansen, R., et al. (2008). The RNA polymerase "switch region" is a target for inhibitors. Cell *135*, 295–307.

Niu, W., Kim, Y., Tau, G., Heyduk, T., and Ebright, R.H. (1996). Transcription activation at class II CAP-dependent promoters: two interactions between CAP and RNA polymerase. Cell *87*, 1123–1134.

Otwinowski, Z., and Minor, W. (1997). Processing of X-ray diffraction data collected in oscillation mode. Methods Enzymol. *276*, 307–326.

Pfleiderer, C., Smid, A., Bartsch, I., and Grummt, I. (1990). An undecamer DNA sequence directs termination of human ribosomal gene transcription. Nucleic Acids Res. *18*, 4727–4736.

Ploeser, J.M., and Loring, H.S. (1949). The ultraviolet absorption spectra of the pyrimidine ribonucleosides and ribonucleotides. J. Biol. Chem. *178*, 431–437.

Qi, Y., and Hulett, F.M. (1998). PhoP∼P and RNA polymerase σA holoenzyme are sufficient for transcription of Pho regulon promoters in *Bacillus subtilis*: PhoP∼P activator sites within the coding region stimulate transcription in vitro. Mol. Microbiol. *28*, 1187–1197.

Revyakin, A., Liu, C., Ebright, R.H., and Strick, T.R. (2006). Abortive initiation and productive initiation by RNA polymerase involve DNA scrunching. Science *314*, 1139–1143.

Sagitov, V., Nikiforov, V., and Goldfarb, A. (1993). Dominant lethal mutations near the 5′ substrate binding site affect RNA polymerase propagation. J. Biol. Chem. *268*, 2195–2202.

Sambrook, J., and Russell, D. (2001). Molecular Cloning: A Laboratory Manual (Cold Spring Harbor, NY: Cold Spring Harbor Laboratory).

Sancar, A., Stachelek, C., Konigsberg, W., and Rupp, W.D. (1980). Sequences of the *recA* gene and protein. Proc. Natl. Acad. Sci. USA *77*, 2611–2615.

Sarkar, S., Ma, W.T., and Sandri, G.H. (1992). On fluctuation analysis: a new, simple and efficient method for computing the expected number of mutants. Genetica *85*, 173–179.

Schreiber, E., Matthias, P., Müller, M.M., and Schaffner, W. (1989). Rapid detection of octamer binding proteins with 'mini-extracts', prepared from a small number of cells. Nucleic Acids Res. *17*, 6419.

Sergio, S., Pirali, G., White, R., and Parenti, F. (1975). Lipiarmycin, a new antibiotic from *Actinoplanes* III. Mechanism of action. J. Antibiot. (Tokyo). *28*, 543–549.

Severinov, K., Mooney, R., Darst, S.A., and Landick, R. (1997). Tethering of the large subunits of *Escherichia coli* RNA polymerase. J. Biol. Chem. *272*, 24137–24140.

Sosunov, V., Zorov, S., Sosunova, E., Nikolaev, A., Zakeyeva, I., Bass, I., Goldfarb, A., Nikiforov, V., Severinov, K., and Mustaev, A. (2005). The involvement of the aspartate triad of the active center in all catalytic activities of multisubunit RNA polymerase. Nucleic Acids Res. *33*, 4202–4211.

Srivastava, A., Talaue, M., Liu, S., Degen, D., Ebright, R.Y., Sineva, E., Chakraborty, A., Druzhinin, S.Y., Chatterjee, S., Mukhopadhyay, J., et al. (2011). New target for inhibition of bacterial RNA polymerase: 'switch region'. Curr. Opin. Microbiol. *14*, 532–543.

Srivastava, A., Degen, D., Ebright, Y.W., and Ebright, R.H. (2012). Frequency, spectrum, and nonzero fitness costs of resistance to myxopyronin in *Staphylococcus aureus*. Antimicrob. Agents Chemother. *56*, 6250–6255.

Strong, M., Sawaya, M.R., Wang, S., Phillips, M., Cascio, D., and Eisenberg, D. (2006). Toward the structural genomics of complexes: crystal structure of a PE/PPE protein complex from *Mycobacterium tuberculosis*. Proc. Natl. Acad. Sci. USA *103*, 8060–8065.

Summers, B.B., Beavers, J.W., and Klibanov, O.M. (2014). Sofosbuvir, a novel nucleotide analogue inhibitor used for the treatment of hepatitis C virus. J. Pharm. Pharmacol. *66*, 1653–1666.

Svetlov, V., Vassylyev, D.G., and Artsimovitch, I. (2004). Discrimination against deoxyribonucleotide substrates by bacterial RNA polymerase. J. Biol. Chem. *279*, 38087–38090.

Sweetser, D., Nonet, M., and Young, R.A. (1987). Prokaryotic and eukaryotic RNA polymerases have homologous core subunits. Proc. Natl. Acad. Sci. USA *84*, 1192–1196.

Tang, H., Severinov, K., Goldfarb, A., Fenyo, D., Chait, B., and Ebright, R.H. (1994). Location, structure, and function of the target of a transcriptional activator protein. Genes Dev. *8*, 3058–3067.

Temiakov, D., Zenkin, N., Vassylyeva, M.N., Perederina, A., Tahirov, T.H., Kashkina, E., Savkina, M., Zorov, S., Nikiforov, V., Igarashi, N., et al. (2005). Structural basis of transcription inhibition by antibiotic streptolydigin. Mol. Cell *19*, 655–666.

Tuske, S., Sarafianos, S.G., Wang, X., Hudson, B., Sineva, E., Mukhopadhyay, J., Birktoft, J.J., Leroy, O., Ismail, S., Clark, A.D., Jr., et al. (2005). Inhibition of bacterial RNA polymerase by streptolydigin: stabilization of a straight-bridge-helix active-center conformation. Cell *122*, 541–552.

Vagin, A., and Teplyakov, A. (1997). MOLREP: an automated program for molecular replacement. J. Appl. Cryst. *30*, 1022–1025.

Vrentas, C.E., Gaal, T., Ross, W., Ebright, R.H., and Gourse, R.L. (2005). Response of RNA polymerase to ppGpp: requirement for the ω subunit and relief of this requirement by *DksA*. Genes Dev. *19*, 2378–2387.

Wang, D., Meier, T.I., Chan, C.L., Feng, G., Lee, D.N., and Landick, R. (1995). Discontinuous movements of DNA and RNA in RNA polymerase accompany formation of a paused transcription complex. Cell *81*, 341–350.

Weinzierl, R.O. (2010). The nucleotide addition cycle of RNA polymerase is controlled by two molecular hinges in the Bridge Helix domain. BMC Biol. *8*, 134.

White, R.L., Burgess, D.S., Manduru, M., and Bosso, J.A. (1996). Comparison of three different in vitro methods of detecting synergy: time-kill, checkerboard, and E test. Antimicrob. Agents Chemother. *40*, 1914–1918.

Yuzenkova, Y., Roghanian, M., and Zenkin, N. (2012). Multiple active centers of multi-subunit RNA polymerases. Transcription *3*, 115–118.

Zhang, Y., Feng, Y., Chatterjee, S., Tuske, S., Ho, M.X., Arnold, E., and Ebright, R.H. (2012). Structural basis of transcription initiation. Science *338*, 1076–1080.

Zhang, Y., Degen, D., Ho, M.X., Sineva, E., Ebright, K.Y., Ebright, Y.W., Mekler, V., Vahedian-Movahed, H., Feng, Y., Yin, R., et al. (2014). GE23077 binds to the RNA polymerase 'i' and 'i+1' sites and prevents the binding of initiating nucleotides. eLife *3*, e02450.

STAR★METHODS

KEY RESOURCES TABLE

REAGENT or RESOURCE	SOURCE	IDENTIFIER
Bacterial and Virus Strains		
Bacillus subtilis MH5636	Qi and Hulett, 1998	N/A
Bacillus subtilis MH5636-Q469R	this paper	N/A
Enterococcus faecium ATCC 19434	ATCC	ATCC 19434
Escherichia coli BL21(DE3)	Invitrogen/ ThermoFisher	Cat# C600003
Escherichia coli D21f2tolC	Fralick and Burns-Keliher, 1994	N/A
Escherichia coli D21f2tolC *rpoB-D516V*	Zhang et al., 2014	N/A
Escherichia coli D21f2tolC *rpoB-H526D*	Zhang et al., 2014	N/A
Escherichia coli D21f2tolC *rpoB-H526Y*	Zhang et al., 2014	N/A
Escherichia coli D21f2tolC *rpoB-S531L*	Zhang et al., 2014	N/A
Escherichia coli D21f2tolC *rpoB-E565D*	this paper	N/A
Escherichia coli D21f2tolC *rpoB-E565G*	this paper	N/A
Escherichia coli D21f2tolC *rpoB-D675A*	Degen et al., 2014	N/A
Escherichia coli D21f2tolC *rpoB-N677K*	Degen et al., 2014	N/A
Escherichia coli D21f2tolC *rpoB-Y1251F*	Degen et al., 2014	N/A
Escherichia coli D21f2tolC *rpoB-Q1256E*	Degen et al., 2014	N/A
Escherichia coli D21f2tolC *rpoB-Q1256L*	Degen et al., 2014	N/A
Escherichia coli D21f2tolC *rpoB-V1275M*	Degen et al., 2014	N/A
Escherichia coli D21f2tolC *rpoB-L1291F*	Degen et al., 2014	N/A
Escherichia coli D21f2tolC *rpoC-R337H*	Degen et al., 2014	N/A
Escherichia coli D21f2tolC *rpoC-R337S*	Degen et al., 2014	N/A
Escherichia coli D21f2tolC *rpoC-K345N*	Degen et al., 2014	N/A
Escherichia coli D21f2tolC *rpoC-K345R*	Degen et al., 2014	N/A
Escherichia coli D21f2tolC *rpoC-R738P*	Degen et al., 2014	N/A
Escherichia coli D21f2tolC *rpoC-A779V*	Degen et al., 2014	N/A
Escherichia coli D21f2tolC *rpoC-G782A*	Degen et al., 2014	N/A
Escherichia coli D21f2tolC *rpoC-G1354S*	Degen et al., 2014	N/A
Escherichia coli XE54	Tang et al., 1994	N/A
Haemophilus influenzae L3296	NAICONS/ Gruppo Lepetit	N/A
Moraxella catarrhalis L3294	NAICONS/ Gruppo Lepetit	N/A
Staphylococcus aureus ATCC 12600	ATCC	ATCC 12600
Staphylococcus aureus ATCC 12600-S531L	Srivastava et al., 2011	N/A
Staphylococcus aureus BAA-1707	ATCC	ATCC BAA-1707
Staphylococcus aureus CB1616	Friedman et al., 2006	N/ A
Staphylococcus aureus NRS1	NARSA	NRS1
Staphylococcus aureus NRS120	BEI Resources	NR-45925
Staphylococcus aureus VRS1	NARSA	VRS1
Staphylococcus simulans M22	NAICONS	N/A
Streptococcus pneumoniae L44	NAICONS/ Gruppo Lepetit	N/A
Streptococcus pneumoniae L899	NAICONS/ Gruppo Lepetit	N/A
Streptococcus pneumoniae L1407	NAICONS/ Gruppo Lepetit	N/A
Streptococcus pneumoniae L1542	NAICONS/ Gruppo Lepetit	N/A
Streptococcus pneumoniae L2868	NAICONS/ Gruppo Lepetit	N/A
Streptococcus pneumoniae L3909	NAICONS/ Gruppo Lepetit	N/A
Streptococcus pneumoniae ND061311	NAICONS/ Gruppo Lepetit	N/A

(*Continued on next page*)

Continued

REAGENT or RESOURCE	SOURCE	IDENTIFIER
Streptococcus pyogenes L49	NAICONS/ Gruppo Lepetit	N/A
Streptococcus pyogenes C203	ATCC	ATCC 12384
Streptococcus pyogenes 12344	ATCC	ATCC 12344
Streptococcus pyogenes 12344 *rpoB*-V135F	this paper	N/A
Streptococcus pyogenes 12344 *rpoB*-S472P	this paper	N/A
Streptococcus pyogenes 12344 *rpoB*-Q473K	this paper	N/A
Streptococcus pyogenes 12344 *rpoB*-Q473R	this paper	N/A
Streptococcus pyogenes 12344 *rpoB*-D476N	this paper	N/A
Streptococcus pyogenes 12344 *rpoB*-D476V	this paper	N/A
Streptococcus pyogenes 12344 *rpoB*-D476Y	this paper	N/A
Streptococcus pyogenes 12344 *rpoB*-S482L	this paper	N/A
Streptococcus pyogenes 12344 *rpoB*-H486Y	this paper	N/A
Streptococcus pyogenes 12344 *rpoB*-S491F	this paper	N/A
Streptococcus pyogenes 12344 *rpoB*-S491Y	this paper	N/A
Streptococcus pyogenes 12344 *rpoB*-G494V	this paper	N/A
Streptococcus pyogenes 12344 *rpoB*-P524L	this paper	N/A
Streptococcus pyogenes 12344 *rpoB*-E525V	this paper	N/A
Streptococcus pyogenes 12344 *rpoB*-M643K	this paper	N/A
Streptococcus pyogenes 12344 *rpoB*-N646I	this paper	N/A
Streptococcus pyogenes 12344 *rpoC*-T791K	this paper	N/A
Streptococcus pyogenes 12344 *rpoC*-T791M	this paper	N/A
Streptococcus pyogenes 12344 *rpoC*-T791R	this paper	N/A
Streptomyces sp. ID38640	this paper	N/A
Streptomyces sp. ID38673	this paper	N/A
Thermus thermophilus HB-8	DSMZ	DSM 579
Chemicals, Peptides, and Recombinant Proteins		
Escherichia coli RNA polymerase σ^{70} core enzyme	this paper	N/A
Escherichia coli RNA polymerase σ^{70} holoenzyme	this paper	N/A
Escherichia coli RNA polymerase σ^{70} holoenzyme	Epicenter	Cat# S90250
Escherichia coli RNA polymerase σ^{70} holoenzyme	Sigma-Aldrich	Cat# R7394
Escherichia coli [531 Ser→Leu]β-RNAP σ^{70} holoenzyme	this paper	N/A
Escherichia coli [565 Glu→Asp]β-RNAP σ^{70} holoenzyme	this paper	N/A
Staphylococcus aureus RNAP σ^{A} holoenzyme	this paper	N/A
Bacillus subtilis [469 (513) Gln→Arg]β-RNAP σ^{A} holoenzyme	this paper	N/A
Thermus thermophilus RNAP σ^{A} holoenzyme	this paper	N/A
HeLaScribe Nuclear Extract	Promega	Cat# E309A
SP6 RNA polymerase	Promega	Cat# P1081
T7 RNAP	Promega	Cat# P2075
ϕ6 RNA-dependent RNA polymerase	ThermoFisher	Cat# F611S
Taq DNA polymerase	Genscript	Cat# E00007-1000
T4 polynucleotide kinase	New England Biolabs	Cat# M0201S
pseudouridimycin (PUM)	this paper	N/A
desoxy-PUM (PUM derivative **1**)	this paper	N/A
PUM nitrile analog (PUM derivative **2**)	this paper	N/A
PUM carboxy analog (PUM derivative **3**)	this paper	N/A
PUM benzylamide analog (PUM derivative **4**)	this paper	N/A
PUM diolic intermediate (PUM derivative **5**)	this paper	N/A
PUM phenyl-dioxaborolan analog (PUM derivative **6**)	this paper	N/A

(*Continued on next page*)

Continued

REAGENT or RESOURCE	SOURCE	IDENTIFIER
rifampin	Sigma-Aldrich	Cat# R3501
lipiarmycin A3	BioAustralis	Cat# BIA-F1356
myxopyronin B	Ebright and Ebright, 2012	N/A
streptolydigin	Sourcon-Padena	PNU-0005481
CBR703	Maybridge	RF05117SC
salinamide A	Degen et al., 2014	N/A
GE23077	Ciciliato et al., 2004	N/A
[2-^{14}C]-thymidine	Hartmann Analytic	Cat# MC 104
[5-^{3}H]-uridine	Hartmann Analytic	Cat# MT 602
L-[^{14}C(U)]-isoleucine	Hartmann Analytic	Cat# ARC 0672
[γ^{32}P]ATP	PerkinElmer	Cat# BLU503H250UC
[α^{32}P]GTP	PerkinElmer	Cat# BLU506H250UC
[α^{32}P]UTP	PerkinElmer	Cat# BLU507H250UC
[α^{32}P]CTP	PerkinElmer	Cat# BLU508H250UC
3′-O-methyl-UTP	RiboMed	N/A
3′-O-methyl-CTP	RiboMed	N/A
3′-O-methyl-GTP	RiboMed	N/A
3′-O-methyl-ATP	RiboMed	N/A
CMPcPP	Jena Biosciences	Cat# NU-438S
GpA	TriLink	Cat# O-31009
dNTP mix	Agilent/ Stratagene	Cat# 200415
BTT agar	Donadio et al., 2009	N/A
Haemophilus Test Medium	Barry et al., 1993	N/A
LB broth	Sambrook and Russell, 2001	N/A
LB agar	Sambrook and Russell, 2001	N/A
Mueller Hinton II cation-adjusted broth	BD Biosciences	Cat# 212322
Todd Hewitt broth	BD Biosciences	Cat# 249240
ampicillin	Sigma-Aldrich	Cat# A0166
pencillin-streptomycin	GIBCO / ThermoFisher	Cat# 15140122
fetal bovine serum albumin	GIBCO / ThermoFisher	Cat# 10437010
human serum	Sigma-Aldrich	Cat# H4522
IPTG	Gold Biotechnology	Cat# I2481C50
lysozyme	Sigma-Aldrich	Cat# L7651
polyethyleneimine (Polymin P)	Sigma-Aldrich	Cat# P3143
human placental DNA	Sigma-Aldrich	Cat# D7011
Filtersafe scintillation fluid	Zinnser Analytic	N/A
Scintiverse BD cocktail	Fisher	Cat# SX18-4
(2R,3R)-(-)-2,3-butanediol	Sigma-Aldrich	Cat# 237639-5G
β-D-pseudouridine	Berry & Associates	Cat# PYA 11080
2,2-dimethoxypropane	Sigma-Aldrich	Cat# D136808
methanesulfonyl chloride	Sigma-Aldrich	Cat# 471259
trimethylphosphine in tetrahydrofuran	Sigma-Aldrich	Cat# 324108
Fmoc chloride	Sigma-Aldrich	Cat# 160512
N,N'-dicyclohexylcarbodiimide	Sigma-Aldrich	Cat# D80002
1-hydroxybenzotriazole	Sigma-Aldrich	Cat# 157260
3,5-dimethylpyrazole-1-carboxamidine	Sigma-Aldrich	Cat# D182257
Critical Commercial Assays		
HeLaScribe Nuclear Extract in vitro Transcription System	Promega	Cat# E3110
QuikChange II site-directed mutagenesis kit	Agilent	Cat# 200523

(*Continued on next page*)

Continued

REAGENT or RESOURCE	SOURCE	IDENTIFIER
Wizard Genomic DNA Purification Kit	Promega	Cat# A1125
Gel/PCR DNA Fragments Extraction Kit	IBI Scientific	Cat# IB47030
Deposited Data		
Streptomyces sp. ID38640	this paper	DSMZ: DSM 26212
Streptomyces sp. ID38640 16S RNA gene sequence	this paper	GI: JQ929050
Streptomyces sp. ID38673 16S RNA gene sequence	this paper	GI: JQ929051
RPo-GpA-PUM structure	this paper	PDB: 5X21
RPo-GpA-CMPcPP structure	this paper	PDB: 5X22
Experimental Models: Cell Lines		
HeLa	ATCC	ATCC CCL-2
Experimental Models: Organisms/Strains		
Female ICR mice, 23-25 g	Harlan Laboratories Italy	N/A
Oligonucleotides		
recA promoter DNA fragments, see Table S4	this paper	N/A
bacteriophage T4 N25 promoter DNA fragment, see Table S4	Revyakin et al., 2006	N25-100-tR2
Cy5-labeled *lacUV5* promoter DNA fragment, see Table S4	Mukhopadhyay et al., 2008	Cy5-*lacUV5*-[-40;+15]
nontemplate-strand, template-strand, and RNA oligos for transcription-elongation-complex scaffolds, see Table S5	IDT	N/A
HeLaScribe Positive Control DNA Fragment	Promega	Cat# E3621
poly(A) ssRNA	GE Healthcare	Cat# 27411001
poly(U-15) ssRNA	Sigma-Aldrich	N/A
S. pyogenes rpoB primers, see Table S4	IDT	N/A
S. pyogenes rpoC primers, see Table S4	IDT	N/A
Recombinant DNA		
pCDFω	Vrentas et al., 2005	N/A
pEcABC-H6	Hudson et al., 2009	N/A
pGEM-3Z	Promega	Cat# P2151
pHrP2x	Pfleiderer et al., 1990	N/A
pREII-NHα	Niu et al., 1996	N/A
pRL663	Wang et al., 1995	N/A
pRL663-786K	this paper	N/A
pRL663-786M	this paper	N/A
pRL663-786R	this paper	N/A
pRL663-788M	Tuske et al., 2005	N/A
pRL663-1139L	Tuske et al., 2005	N/A
pRL663-1139R	Tuske et al., 2005	N/A
pRL706	Severinov et al., 1997	N/A
pRL706-543V	Tuske et al., 2005	N/A
pRL706-545C	Tuske et al., 2005	N/A
pRL706-552M	Feng et al., 2015	N/A
pRL706-531L	this paper	N/A
pRL706-565D	Zhang et al., 2014	N/A
pRL706-565G	this paper	N/A
pRL706-565V	this paper	N/A
pRL706-566C	Zhang et al., 2014	N/A
pRL706-566R	Zhang et al., 2014	N/A
pRL706-566S	Zhang et al., 2014	N/A

(*Continued on next page*)

Continued

REAGENT or RESOURCE	SOURCE	IDENTIFIER
pRL706-618L	Feng et al., 2015	N/A
pRL706-642F	Feng et al., 2015	N/A
pRL706-654H	Feng et al., 2015	N/A
pRL706-657I	Feng et al., 2015	N/A
pRL706-681K	this paper	N/A
pRL706-684I	this paper	N/A
pRL706-684K	Zhang et al., 2014	N/A
pRL706-684T	Zhang et al., 2014	N/A
pCOLADuet-Sau-BC	Srivastava et al., 2011	N/A
pACYCDuet-Sau-H10-A	Srivastava et al., 2011	N/A
pCDFDuet-Sau-Z	Srivastava et al., 2011	N/A
pET21a-Sau-H6-sigA	Srivastava et al., 2011	N/A
pET28a-Tt-σ^A	Zhang et al., 2012	N/A
pUC18	Clontech/ Takara	Cat # 3218
pUC19	Clontech/ Takara	Cat # 3219
pVAI	Dean and Berk, 1988	N/A
Software and Algorithms		
Coot	Emsley et al., 2010	https://www2.mrc-lmb.cam.ac.uk/personal/pemsley/coot/
Fluctuation Analysis Calculator (FALCOR)	Hall et al., 2009	http://www.keshavsingh.org/protocols/FALCOR.html
HKL2000	Otwinowski and Minor, 1997	http://www.hkl-xray.com/
Molrep	Vagin and Teplyakov, 1997	http://www.ccp4.ac.uk/html/molrep.html
SigmaPlot	Systat Software	https://systatsoftware.com/products/sigmaplot/
Phenix	Adams et al., 2010	https://www.phenix-online.org/
UCLA MBI Diffraction Anistropy server	Strong et al., 2006	http://services.mbi.ucla.edu/anisoscale/
US EPA LC50 Model System	Hamilton et al., 1977	http://sdi.odu.edu/model/lc50.php
Other		
ÄKTApurifier 10 FPLC system	GE Healthcare	Cat# 28406264
HiLoad 16/60 Superdex 200 column	GE Healthcare	Cat# 17-1069-01
HiPrep Heparin FF 16/10 column	GE Healthcare	Cat# 28-9365-49
Mono Q 10/100 GL column	GE Healthcare	Cat# 17-5167-01
Mono S HR 10/10 column	GE Healthcare	Cat# 17-0557-01
SP Sepharose FF column	GE Healthcare	Cat# 17-0729-01
Ni-NTA agarose	QIAGEN	Cat# 30230
Combiflash Rf flash liquid chromatography system	Teledyne Isco	Cat# 68-5230-015
30 g C18 RediSep Rf column	Teledyne Isco	Cat# 69-2203-335
Shimadzu series 10 HPLC system with SPD-M10Avp diode array detector	Shimadzu	N/A
Symmetry Shield RP8 HPLC column (250 × 4.6 mm)	Waters	Cat# WAT200670
Agilent 1100 HPLC system with UV detector	Agilent	N/A
Atlantis HPLC column (3 μm; 50 × 4.6 mm)	Waters	Cat# 186003726
HP5985B GC/MS system	Hewlett-Packard	N/A
Esquire 3000 Plus mass spectrometer	Bruker	N/A
Exactive mass spectrometer	ThermoFisher	N/A
600 and 400 MHz NMR spectrometer	Bruker	N/A
Synergy 2 microplate reader	BioTek	N/A

(*Continued on next page*)

Continued

REAGENT or RESOURCE	SOURCE	IDENTIFIER
GENios Pro microplate reader	Tecan	N/A
BioFlo 115 fermentor	Eppendorf	Cat# M1369-1102
Anoxomat AN2CTS culture atmosphere system	Advanced Instruments	N/A
TopCount scintillation counter	Packard / PerkinElmer	Cat# C9912V0
Tri-Carb 3110TR liquid scintillation analyzer	PerkinElmer	N/A
LS6500 scintillation counter	Beckman Coulter	N/A
Typhoon 9400 variable mode imager	GE Healthcare	N/A
5% TBE-polyacrylamide slab gels	Bio-Rad	Cat# 456-5013
6%, 10%, or 15% polyacrylamide (19:1 acrylamide: bisacrylamide; 7 M urea) slab gels	Sambrook and Russell, 2001	N/A
Filtermate 96-well UniFilter harvester	Packard / PerkinElmer	Cat# C961961
UniFilter GF/B	PerkinElmer	Cat# 6005177
UniFilter GF/C	PerkinElmer	Cat# 6005174
GF/C glass-microfiber filters	Whatman/ GE Healthcare	Cat# 1822-047
DE81 filter discs	Whatman/ GE Healthcare	Cat# 3658-325
10.25" disc filter paper	Scienceware / Bel-Art	Cat# 146320010
Taxo A differentiation discs	BD Biosciences	Cat# 231042
pyrase strips	Fluka/ Sigma-Aldrich	Cat# 67886
vapor-diffusion hanging drop tray	Hampton Research	Cat# HR3-306

CONTACT FOR REAGENT AND RESOURCE SHARING

Further information and requests for resources and reagents should be directed to and will be fulfilled by Lead Contact, Richard H. Ebright (ebright@waksman.rutgers.edu).

EXPERIMENTAL MODEL AND SUBJECT DETAILS

Mice

Female ICR mice were obtained from Harlan Laboratories, Italy. All mice weighed 23-25 g when tested. Mice were adapted to standardized environmental conditions (temperature = 23±2°C; humidity = 55±10%) for one week prior to infection. Procedures were performed in accordance with the institution's guidelines for the humane handling, care, and treatment of research animals.

Cell line and cell culture

HeLa cells were grown to 70%–80% confluence in DMEM, high-glucose, 2 mM L-glutamine medium containing 10% fetal bovine serum and 1% penicillin-streptomycin. Cells were maintained at 37°C in a 5% CO_2 incubator.

METHOD DETAILS

E. coli RNAP core enzyme

For experiments in Figure 3C, *E. coli* RNAP core enzyme was prepared from *E. coli* strain BL21(DE3) (Invitrogen/ThermoFisher) transformed with plasmids pEcABC-H6 (Hudson et al., 2009) and pCDFω (Vrentas et al., 2005), using culture and induction procedures as in Hudson et al., 2009, and using polyethylenimine precipitation, ammonium-sulfate precipitation, immobilized-metal-ion affinity chromatography on Ni-NTA agarose (QIAGEN), and anion-exchange chromatography on Mono Q (GE Healthcare), as in Mukhopadhyay et al., 2003.

For experiments assessing promoter-independent transcription in Table S1, *E. coli* RNAP core enzyme was prepared from *E. coli* strain XE54 (Tang et al., 1994) transformed with plasmid pRL706 (Severinov et al., 1997), using culture and induction procedures, polyethylenimine precipitation, ammonium-sulfate precipitation, immobilized-metal-ion affinity chromatography on Ni-NTA agarose (QIAGEN), and anion-exchange chromatography on Mono Q (GE Healthcare), as in Niu et al., 1996.

E. coli RNAP σ^{70} holoenzyme

For experiments in Figure 1B, [531Ser→Leu]β-RNAP σ^{70} holoenzyme was prepared from *E. coli* strain XE54 (Tang et al., 1994) transformed with plasmid pRL706-531L [constructed from plasmid pRL706 (Severinov et al., 1997) by use of site-directed mutagenesis

(QuikChange Site-Directed Mutagenesis Kit; Agilent)], using culture and induction procedures, polyethylenimine precipitation, ammonium-sulfate precipitation, immobilized-metal-ion affinity chromatography on Ni-NTA agarose (QIAGEN), and anion-exchange chromatography on Mono Q (GE Healthcare), as in Niu et al., 1996.

For experiments in Figure S3C, *E. coli* RNAP σ^{70} holoenzyme and [565Glu→Asp]β-RNAP σ^{70} holoenzyme were prepared from *E. coli* strain XE54 (Tang et al., 1994) transformed with plasmid pRL706 (Severinov et al., 1997) or pRL706-565D (Zhang et al., 2014), using the same procedures.

For experiments in Figure 3D, *E. coli* RNAP σ^{70} holoenzyme was prepared from *E. coli* strain XE54 (Tang et al., 1994) transformed with plasmid pREII-NHα (Niu et al., 1996), using culture and induction procedures, polyethylenimine precipitation, ammonium-sulfate precipitation, immobilized-metal-ion affinity chromatography on Ni-NTA agarose (QIAGEN), and anion-exchange chromatography on Mono Q (GE Healthcare), as in Degen et al., 2014.

S. aureus RNAP σ^A holoenzyme

S. aureus RNAP core enzyme was prepared from *E. coli* strain BL21(DE3) (Invitrogen/ThermoFisher) transformed with plasmids pCOLADuet-Sau-BC, pACYCDuet-Sau-H10-A, and pCDFDuet-Sau-Z, using polyethylenimine precipitation, ammonium-sulfate precipitation, immobilized-metal-ion affinity chromatography on Ni-NTA agarose (QIAGEN), and cation-exchange chromatography on HiPrep Heparin (GE Healthcare); *S. aureus* σ^A was prepared from *E. coli* strain BL21(DE3) transformed with pET21a-Sau-H6-sigA, using immobilized-metal-ion affinity chromatography on Ni-NTA agarose (QIAGEN) and gel-filtration chromatography on Superdex 200 (GE Healthcare); and *S. aureus* RNAP core enzyme and *S. aureus* σ^A were combined to yield *S. aureus* RNAP σ^A holoenzyme, as in Srivastava et al., 2011.

B. subtilis RNAP σ^A holoenzyme

Rif-resistant *B. subtilis* [469(513)Gln→Arg]β-RNAP σ^A holoenzyme was prepared from *B. subtilis* strain MH5636-Q469R [spontaneous Rif-resistant mutant of *B. subtilis* strain MH5636 (Qi and Hulett, 1998); selected on LB agar containing 2 μg/mL Rif; confirmed by PCR amplification and sequencing of *rpoB*], using immobilized-metal-ion affinity chromatography on Ni-NTA agarose (QIAGEN), as in Qi and Hulett, 1998.

T. thermophilus RNAP σ^A holoenzyme

T. thermophilus RNAP core enzyme was prepared from *T. thermophilus* strain H8 (DSM 579; DSMZ), using polyethylenimine precipitation, ammonium-sulfate precipitation, cation-exchange chromatography on SP Sepharose FF (GE Healthcare), anion-exchange chromatography on Mono Q (GE Healthcare), and cation-exchange chromatography on Mono S (GE Healthcare); *T. thermophilus* σ^A was prepared from *E. coli* strain BL21(DE3) transformed with pET28a-Tt-σ^A, using immobilized-metal-ion affinity chromatography on Ni-NTA agarose (QIAGEN) and anion-exchange chromatography on Mono Q (GE Healthcare); *T. thermophilus* RNAP core enzyme and *T. thermophilus* σ^A were combined to yield *T. thermophilus* RNAP σ^A holoenzyme; and *T. thermophilus* RNAP σ^A holoenzyme was further purified using size-exclusion chromatography on Superdex 200 (GE Healthcare), as in Zhang et al., 2014.

Microbial extract screening

A sub-library of ~3,000 microbial extracts (prepared as in Donadio et al., 2009) with growth-inhibitory activity against *S. aureus* ATCC 6538 was screened for the ability to inhibit *E. coli* RNAP and bacteriophage SP6 RNAP. Screening was performed using 96-well microplates. Reactions contained (50 μL): 5 μL extract (dissolved in 10% DMSO), 0.2 U *E. coli* RNAP σ^{70} holoenzyme (Sigma-Aldrich) or 0.2 U SP6 RNAP (Promega), 0.2 nM plasmid pUC18 (Clontech/Takara; for assays with *E. coli* RNAP) or 0.2 nM plasmid pGEM-3Z (Promega; for assays with SP6 RNAP), 500 μM ATP, 500 μM GTP, 500 μM CTP, and 2 μM [α^{32}P]UTP (0.2 Bq/fmol; PerkinElmer), in 20 mM Tris-acetate (pH 7.9), 50 mM KCl, 4 mM magnesium acetate, 0.1 mM EDTA, 5 mM dithiothreitol, and 100 μg/mL bovine serum albumin. Reaction components except DNA were pre-equilibrated 10 min at 22°C. Reactions were initiated by addition of DNA, were allowed to proceed 1 hr at 22°C, and were terminated by addition of 150 μL ice-cold 10% (w/v) trichloroacetic acid (TCA). After 1 hr at 4°C, resulting TCA precipitates were collected on glass-fiber filters (UniFilter GF/B; PerkinElmer) using a 96-well harvester (Packard/PerkinElmer) and were washed once with water. Radioactivity was quantified using a TopCount scintillation counter (Packard/PerkinElmer), and % inhibition was calculated as:

$$\%\ \text{inhibition} = 100\text{-}\left[100\left(R_{sample}\text{-}R_{neg}\right)/\left(R_{pos}\text{-}R_{neg}\right)\right]$$

where R_{sample}, R_{pos} and R_{neg} are observed radioactivity levels in a reaction, in a control reaction without extract, and in a control reaction without plasmid, respectively.

Two extracts that inhibited the reaction with *E. coli* RNAP by ≥ 80%, that did not inhibit the reaction with SP6 RNAP, and that did not contain mass-spectrometry signals indicative of a previously characterized RNAP inhibitor, were designated as "hit extracts."

Characterization of producer strains

The producer strains of the hit extracts were strains ID38640 and ID38673. ID38640 and ID38673 are Actinobacterial isolates from soil samples collected in Italy and France, respectively. ID38640 and ID38673 exhibit cell morphologies consistent with the genus

Streptomyces and exhibit 16S rRNA gene sequences (determined as in Mazza et al., 2003; GenBank accession numbers GI: JQ929050 and GI: JQ929051) that were 99.9% identical over 1.4 kB to each other and were highly similar to those of a cluster of closely-related *Streptomyces* species (*S. nigrescens*, *S. tubercidicus*, *S. rimosus* subsp. *rimosus*, *S. hygroscopicus* subsp. *angustmyceticus*, and *S. libani* subsp. *libani*).

Isolation and purification of pseudouridimycin

For each producer strain of a hit extract, the strain was cultured on a 55 mm BTT agar (Donadio et al., 2009) plate for 4-7 days at 30°C, the mycelium was scraped from the plate and used to inoculate a 50 mL Erlenmeyer flask containing 15 mL of seed medium (20 g/L dextrose monohydrate, 2 g/L yeast extract, 8 g/L soybean meal, 1 g/L NaCl, and 4 g/L $CaCO_3$, pH 7.3), and the resulting culture was incubated 48 hr at 30°C on a rotary shaker (200 rpm agitation). Following initial incubation, 5 mL of the culture was used to inoculate 100 mL of fresh seed medium in a 500 mL flask, and the resulting culture was incubated 72 hr under the same conditions. A 5% (v/v) inoculum was transferred into 2 L of production medium (10 g/L dextrose monohydrate, 24 g/L maize dextrin, 8 g/L soy peptone, 5 g/L yeast extract, and 1 g/L NaCl, pH 7.2) in a 3-L vessel, and the resulting culture was grown in a BioFlo 115 Fermentor (Eppendorf) 96 hr at 30°C, with aeration at 0.5 volume air per volume medium per min and stirring at 600 rpm. The culture was filtered through 10.25″ disc filter paper (Scienceware/Bel-Art), and the resulting cleared broth was concentrated to ~1 L *in vacuo* and loaded onto a column of 500 mg of Dowex 50W x 400 mesh (previously activated with two bed volumes of 5% HCl and washed with H_2O until neutralization). After washing with 5 bed volumes each of 20 mM sodium acetate at pH 6 and sodium acetate at pH 7, PUM was eluted using six bed volumes of 100 mM NH_4OAc at pH 9. PUM-containing fractions were desalted by reversed-phase medium-pressure liquid chromatography on Combiflash Rf (Teledyne Isco) using a 30 g C18 RediSep Rf column (Teledyne Isco) with linear gradient from 0 to 20% phase B in 20 min (phase A, 0.02% trifluoroacetic acid in H_2O; phase B, acetonitrile) and flow rate of 35 mL/min. PUM-containing fractions were pooled, concentrated, and lyophilized twice to yield 196 mg of a white solid highly soluble in water, DMSO, and methanol.

Structure elucidation of PUM

Ion-trap ESI-MS (Bruker Esquire 3000 Plus) showed a protonated molecular ion at *m/z* 487 $[M+H]^+$ and a bimolecular ion at 973 $[2M+H]^+$ (Figure S1A). Ion-trap ESI-MS/MS (Bruker Esquire 3000 Plus) showed major peaks at *m/z* 334, 353, 371, 389, 452, and 479 $[M+H]^+$. HR-MS (Thermo Fisher Exactive) showed an exact mass of 487.18865, consistent with the molecular formula $C_{17}H_{26}N_8O_9$.

Reversed-phase HPLC (Shimadzu Series 10 with SPD-M10Avp diode array detector; Waters Symmetry Shield RP8 5 μm, 250 × 4.6 mm, column; phase A = 2 mM heptafluorobutyric acid in water; phase B = 2 mM heptafluorobutyric acid in acetonitrile; gradient = 0% B at 0 min, 10% B at 20 min, 95% B at 30 min; flow rate = 1 mL/min) showed a single peak with a retention time of 12 min. The UV-absorbance spectrum showed maxima at 200 nm and 262 nm, consistent with the presence of a pyrimidine moiety (Ploeser and Loring, 1949; Figure S1A).

The ^1H NMR spectrum (600 and 400 MHz Bruker spectrometer in DMSO-d6 at 25°C) revealed one olefinic (H6), five amide (H6′, H3, H5, Hα, and Hε-Gln), four methylene (Hβ-Gln, Hγ-Gln, Hα-Gly, and H5′), and five methine (H1′, H2′, H3′, H4′, and Hα-Gln) signals (Figure S1B). The 2D ^1H–^{13}C-HSQC and -HMBC NMR spectra (600 and 400 MHz Bruker spectrometer in DMSO-d6 at 25°C) identified five carboxyl-amide groups (C2, C4, C = O Gln, C = O Gly, and Cδ-Gln), two olefinic carbons (C1 and C6), four methine carbons belonging to a sugar ring (C1′, C2′, C3′, and C4′), one other methine carbon (Cα-Gln), and four methylene groups (Cα-Gly, Cβ-Gln, Cγ-Gln, and C5′) (Figures S1C and S1D).

The COSY NMR spectrum (600 and 400 MHz Bruker spectrometer in DMSO-d6 at 25°C) identified correlations between the five sugar protons: H1′ (δH 4.35), H2′ (δH 3.92), H3′ (δH 3.65), H4′ (δH 3.65) and H5′ (δH-A 3.24; H-B 3.17). The chemical shift of C5′ and ribose ^{15}N-HSQC correlations between H6′ and H5′ indicated the presence of 6′-amino-ribose. Nitrogen signals N2 and N3 in the N-HSQC spectrum, HMBC correlations of H1′ to C1, C2 and C6, and HMBC correlations of H6 to C1′, C1, C2, and C6, indicated the presence of uracil C-linked to C1′ of 6′-amino-ribose. ^{13}C-NMR spectra and COSY indicated the presence of a glutaminyl moiety, and HMBC correlations of H6′ and the methine at δ_H 4.72 (Hα-Gln) to the carbonyl at δ_c 169.5 indicated linkage of the glutaminyl moiety to N6′ of 6′-amino-ribose. Nε at δ 108.9 was assigned by N-HSQC. The absence of a glutaminyl Nα signal in the N-HSQC spectrum suggested the possible presence of an hydroxamic acid, and this was confirmed by reduction of PUM with aqueous $TiCl_3$ (Mattingly and Miller, 1980) to yield desoxy-PUM (**1** in Figure 5A), exhibiting ion-trap ESI-MS mass of 471 $[M+H]^+$, ion-trap ESI-MS/MS major peaks at *m/z* 355 and 372 $[M+H]^+$, and a new nitrogen peak at δ117.7 in the ^{15}N HSQC spectrum assignable as glutaminyl Nα, with corresponding NH at δH 8.34 coupling with δ_H 4.24 (Hα-Gln). The presence of two protons (Hα1 and Hβ2) coupling to a HN (δ_N 75) in COSY, the HMBC correlations of Hα1 and Hβ2 to a carbonyl at δ_c 157, and a NOESY NMR spectrum (600 MHz Bruker spectrometer in DMSO-d6 at 25°C) of desoxy-PUM indicated the presence of glycine C-linked to glutamine Nα. The chemical shift HN (δ_N 75) with corresponding δ_H 7.43 indicated the presence of formamidine C-linked to glycine Nα.

The stereochemistry of the glutamine residue was established to be (L) by total hydrolysis followed by chiral GC-MS (Hewlett-Packard HP5985B GC-MS; procedures as in Kettenring et al., 1991). The stereochemistry of the ribose sugar was inferred to be D by analogy to the natural product pseudouridine and was confirmed to be D by comparison of a sample of desoxy-PUM prepared by reduction of PUM with $TiCl_3$ to a sample of desoxy-PUM prepared by total synthesis using a D-ribose precursor (Figures 5A and 5B).

Effects of PUM on macromolecular synthesis

Cultures of *Staphylococcus simulans* strain M22 in 0.5x Mueller Hinton II broth (BD Biosciences) were incubated at 37°C with shaking until OD_{600} = 0.5; diluted in the same medium to OD_{600} = 0.1-0.2; supplemented with 6 kBq/mL [2-^{14}C]-thymidine (Hartmann Analytic), 40 kBq/mL [5-^{3}H]-uridine (Hartmann Analytic), or 6 kBq/mL L-[^{14}C(U)]-isoleucine (Hartmann Analytic); and further incubated at 37°C with shaking. After 15 min, cultures were divided into two equal aliquots, PUM was added to one aliquot to a final concentration of 100-200 μM, and cultures were further incubated at 37°C with shaking. At time points 0, 10, 20, and 40 min following addition of PUM, 200 μL aliquots were removed, mixed with 2 mL ice-cold 10% TCA containing 1 M NaCl, and incubated 30-60 min on ice. The resulting TCA precipitates were collected by filtration on glass-microfiber filters (GF/C; Whatman/GE Healthcare), and filters were washed with 5 mL 2.5% TCA containing 1 M NaCl, transferred to scintillation vials, and dried. Filtersafe scintillation fluid was added (2 mL; Zinnser Analytic), and radioactivity was quantified by scintillation counting (Tri-Carb 3110TR Liquid Scintillation Analyzer; PerkinElmer).

RNAP-inhibitory activity in vitro

For experiments in Figure 1B and Table S1 assessing promoter-dependent transcription by *E. coli* RNAP and *S. aureus* RNAP, reaction mixtures contained (25 μL): 0-20 μM PUM, RNAP [1 U *E. coli* RNAP σ^{70} holoenzyme (Epicentre), 20 nM *E. coli* [531Ser→Leu]β-RNAP σ^{70} holoenzyme, or 20 nM *S. aureus* σ^{A} RNAP holoenzyme], 10 nM DNA fragment carrying positions −112 to −1 of *E. coli recA* promoter (Sancar et al., 1980) followed by transcribed-region positions +1 to +363 of HeLaScribe Positive Control DNA (Promega; sequence at https://www.ncbi.nlm.nih.gov/pmc/articles/PMC4021065/bin/1471-2199-15-7-S1.docx; yields 363 nt transcript), 20 μM [α^{32}P]GTP (0.3 Bq/fmol; PerkinElmer), 400 μM ATP, 400 μM CTP, and 6.25 μM UTP (6.25 μM, 50 μM, or 250 μM UTP for Table S1), in 10 mM Tris-HCl (pH. 7.8), 2 mM HEPES-NaOH, 40 mM KCl, 3 mM $MgCl_2$, 0.2 mM dithiothreitol, 0.09 mM EDTA, 0.2 mM phenylmethylsulfonyl fluoride, and 10% glycerol. Reaction components except RNAP were pre-equilibrated 10 min at 30°C. Reactions were initiated by addition of RNAP, were allowed to proceed 15 min at 30°C, and were terminated by addition of 175 μL HeLa Extract Stop Solution (Promega). Samples were phenol extracted and ethanol precipitated (procedures as in Sambrook and Russell, 2001), and pellets were resuspended in 10 μL 47.5% formamide, 10 mM EDTA, 0.025% bromophenol blue, and 0.01% xylene cyanol and heated 5 min at 95°C. Products were applied to denaturing 6% polyacrylamide (19:1 acrylamide:bisacrylamide; 7 M urea) slab gels (Sambrook and Russell, 2001), and gels were electrophoresed in TBE (Sambrook and Russell, 2001) at 10 V/cm for 1.5 hr, dried using a gel dryer (Bio-Rad), and analyzed by storage-phosphor imaging (Typhoon; GE Healthcare).

For experiments in Figure 1B and Table S1 assessing promoter-dependent transcription by human RNAP I, human RNAP II, and human RNAP III, reaction mixtures contained (25 μL): 0-80 μM PUM, HeLa nuclear extract [3 μL HeLa nuclear extract prepared as in Schreiber et al., 1989, using ~4x10^{7} HeLa cells grown to 70%–80% confluence in DMEM, high glucose, 2 mM L-glutamine medium containing 10% fetal bovine serum (GIBCO/ThermoFisher) and 1% penicillin-streptomycin (GIBCO/ThermoFisher) for assays of human RNAP I; or 6 U HeLaScribe Nuclear Extract (Promega) for assays of human RNAP II and human RNAP III], promoter DNA [4 nM EcoRI-linearized plasmid pHrP2x (Pfleiderer et al., 1990) carrying human rDNA promoter for assays of human RNAP I (yields 379 nt transcript); 20 nM HeLaScribe Positive Control DNA (Promega) carrying cytomegalovirus immediate early promoter for assays of human RNAP II (yields 363 nt transcript with same sequence as *E.-coli*-RNAP-dependent transcript of preceding paragraph); or 2 nM plasmid pVAI (Dean and Berk, 1988) carrying adenovirus VAI promoter for assays of human RNAP III (yields 160 nt transcript)], 20 μM [α^{32}P]GTP (0.3 Bq/fmol: PerkinElmer), 400 μM ATP, 400 μM CTP, and 6.25, 50, or 250 μM UTP, in transcription buffer [12 mM HEPES-NaOH (pH 7.9), 75 mM KCl, 5 mM $MgCl_2$, 10 mM creatine phosphate, 0.5 mM dithiothreitol, 0.1 mM EDTA, and 12% glycerol, for assays with human RNAP I; 10 mM Tris-HCl (pH 7.8), 2 mM HEPES-NaOH, 44 mM KCl, 3 mM $MgCl_2$, 0.2 mM dithiothreitol, 0.09 mM EDTA, 0.2 mM phenylmethylsulfonyl fluoride, and 10% glycerol, for assays with human RNAP II and human RNAP III]. Procedures were as in the preceding paragraph.

For experiments in Figure 1B assessing transcription by *B. subtilis* RNAP, SP6 RNAP, and T7 RNAP, reaction mixtures contained (50 μL): 0-200 μM PUM, RNAP [0.2 U *B. subtilis* [469(513)Gln→Arg]β-RNAP σ^{A} holoenzyme (units defined as in Qi and Hulett, 1998), 0.2 U SP6 RNAP (Promega), or 0.2 U T7 RNAP (Promega)], DNA [0.2 nM plasmid pUC18 (Clontech; for assays with *B. subtilis* RNAP) or 0.2 nM plasmid pGEM-3Z (Promega; for assays with SP6 RNAP and T7 RNAP)], 500 μM ATP, 500 μM GTP, 500 μM CTP, and 6.25 μM [α^{32}P]UTP (0.2 Bq/fmol; PerkinElmer; 6.25, 50, or 250 μM for Table S1), in 40 mM Tris-HCl (pH 7.9), 6 mM $MgCl_2$, 2 mM spermidine, 10 mM NaCl, 10 mM dithiothreitol, and 10 μg/mL bovine serum albumin. Reaction components except DNA were pre-equilibrated 15 min at 37°C. Reactions were initiated by addition of DNA, were allowed to proceed 15 min at 37°C, and were terminated by addition of 150 μL ice-cold 10% (w/v) TCA. After 30 min on ice, the resulting TCA precipitates were collected on glass-fiber filters (UniFilter GF/C; PerkinElmer) using a 96-well harvester (Packard/PerkinElmer). filters were washed once with water, and radioactivity was quantified using a TopCount scintillation counter (Packard/PerkinElmer).

For experiments in Figure 1B assessing transcription by ϕ6 RNA-dependent RNAP, reaction mixtures contained (20 μL): 0-400 μM PUM, 0.5 U ϕ6 RNAP (Thermo Fisher), 2 μg poly(A) ssRNA (GE Healthcare), 1 μM poly(U-15) ssRNA primer (Sigma-Aldrich), 400 μM ATP, 400 μM GTP, 400 μM CTP, and 1.56 μM [α^{32}P]UTP (0.02 Bq/fmol; PerkinElmer) in 50 mM Tris-acetate (pH 8.7), 50 mM ammonium acetate, and 1.5 mM $MnCl_2$. Reaction components other than RNA template, RNA primer, and NTPs were pre-incubated 10 min at 30°C. Reactions were initiated by addition of RNA template, RNA primer, and NTPs, reactions were allowed to proceed 1 hr at 30°C, and reactions were terminated by spotting on DE81 filter discs (Whatman; pre-wetted with water) and incubating 1 min at 22°C. Filters were washed with 3x3 mL 0.5 M sodium phosphate dibasic, 2x3 mL water, and 3 mL ethanol using a filter manifold

(Hoefer); filters were placed in scintillation vials containing 10 mL Scintiverse BD Cocktail (ThermoFisher); and radioactivity was quantified by scintillation counting (LS6500; Beckman-Coulter).

For experiments in Table S1 assessing promoter-independent transcription by *E. coli* RNAP and HeLa nuclear extract (human RNAP I/II/II), reaction mixtures contained (20 μL): 0-100 μM PUM, 100 nM *E. coli* RNAP core enzyme or 8 U HeLaScribe Nuclear Extract (Promega), 1 μg human placental DNA (Sigma-Aldrich; catalog number D7011), 400 μM ATP, 400 μM GTP, and 400 μM CTP, and 1.56, 25, or 400 μM [α^{32}P]UTP (0.1-1 Bq/fmol; PerkinElmer), in 40 mM Tris-HCl (pH 8.0), 7 mM HEPES-NaOH, 70 mM ammonium sulfate, 30 mM KCl, 12 mM $MgCl_2$, 5 mM dithiothreitol, 0.1 mM EDTA, and 12% glycerol. Procedures were as in Degen et al., 2014. Reaction components other than DNA and NTPs were pre-incubated 10 min at 30°C, DNA was added, and reaction components other than NTPs were incubated 15 min at 30°C. Reactions were initiated by addition of NTPs, reactions were allowed to proceed 1 hr at 30°C, and reactions were terminated by spotting on DE81 filter discs (Whatman; pre-wetted with water) and incubating 1 min at 22°C. Filters were washed, and radioactivity on filters was quantified, as in the preceding paragraph.

For experiments in Figures S3C and 5C, fluorescence-detected transcription assays were performed as in Zhang et al., 2014.

Half-maximal inhibitory concentrations (IC_{50}s) were calculated by non-linear regression in SigmaPlot (Systat Software).

Antibacterial activity in vitro

Antibacterial activities in vitro (Figure 1C, rows 1-20; Figure 5D) were determined using broth-microdilution growth-curve assays (Holowachuk et al., 2003). [PUM degrades in phosphate-containing media with a half-life of ~12 hr. Broth-microdilution endpoint assays (CLSI/NCCLS, 2009), which have a run time of 16-24 hr (CLSI/NCCLS, 2009), which corresponds to 1.3 to 2 PUM half-lives, underestimate absolute antibacterial activities of PUM. Broth-microdilution growth-curve assays (Holowachuk et al., 2003), which have shorter run times between assay start and assay signal, more accurately estimate absolute antibacterial activities of PUM.] Colonies of the indicated bacterial strains (5 to 10 per strain) were suspended in 3 mL phosphate-buffered saline (Sambrook and Russell, 2001), suspensions were diluted to $1x10^5$ cfu/mL with growth medium [Todd Hewitt broth (BD Biosciences) for *S. pyogenes* and *S. pneumoniae*, aged Mueller Hinton II cation-adjusted broth (BD Biosciences; autoclaved and allowed to stand 2-12 months at room temperature before use) for *Staphylococcus aureus* and *Enterococcus faecium,* fresh Mueller Hinton II cation-adjusted broth (autoclaved and used immediately) for *Moraxella catarrhalis*, or fresh Mueller Hinton II cation-adjusted broth (BD Biosciences; autoclaved and used immediately) containing 0.4% *Haemophilus* Test Medium (Barry et al., 1993) and 0.5% yeast extract for *Haemophilus influenzae*], 50 μL aliquots were dispensed into wells of a 96-well microplate containing 50 μL of the same medium or 50 μL of a 2-fold dilution series of PUM in the same medium (final concentrations = 0 and 0.25-256 μM), plates were incubated at 37°C with shaking, and optical densities at 600 nm were recorded at least hourly using a Synergy 2 (BioTek) or GENios Pro (Tecan) microplate reader. For each dilution series, growth curves were plotted, areas under growth curves were calculated, and IC_{50} was extracted as the lowest tested concentration of PUM that reduced area under the growth curve to 50% that in the absence of PUM (using only time points for rise phase of the growth curve in the absence of PUM).

Identical results were obtained in assays in the absence and presence of 30% human serum (Sigma-Aldrich; Figure 1C, rows 1-4), indicating that PUM does not bind tightly to human serum proteins (unbound fraction ~100%).

Cytotoxicities for human macrovascular endothelial cells and human monocytes in culture (Figure 1C, rows 21-22) were determined as in Mazzetti et al., 2012.

Antibacterial activity in vivo

Antibacterial activity in vivo was assessed in a mouse *S. pyogenes* peritonitis model (Figure 1D; Table S2). Female ICR mice (weight = 23-25 g; Harlan Laboratories Italy) were adapted to standardized environmental conditions (temperature = 23±2°C; humidity = 55±10%) for one week prior to infection. Infection was induced by intraperitoneal injection of 0.5 mL saline solution (supplemented with 1% peptone) containing 4×10^3 cfu *S. pyogenes* C203 (an inoculum resulting in ≥ 95% mortality in untreated controls within 48 to 72 hr after infection). Infected mice (eight mice per group; number determined by power calculations; assigned randomly to groups; unblinded) were treated with either: (i) 0.2 mL 5% dextrose or 0.2 mL of a 2.5-fold dilution series of PUM in 5% dextrose, administered intravenously 10 min after infection and again 6 hr after infection (total PUM dose = 0 or 3.2-50 mg/kg), (ii) 0.25 mL 5% dextrose or 0.25 mL of a 2.5-fold dilution series of PUM in 5% dextrose, administered intravenously 10 min after infection (total PUM dose = 0 or 1.024-40 mg/kg), or (iii) 0.25 mL 5% dextrose or 0.25 mL of a 2.5-fold dilution series of PUM in 5% dextrose, administered subcutaneously 10 min after infection (total PUM dose = 0 or 1.024-40 mg/kg). Survival was monitored for 7 days after infection. Experiments were performed in compliance with vertebrate animal ethical regulations and with Institutional Animal Care and Use Committee (IACUC) approval.

ED_{50}s (doses yielding 50% survival at 7 days) and 95% confidence limits were calculated using the trimmed Spearman-Karber method as implemented in the US EPA LC50 Model System (Hamilton et al., 1977; http://sdi.odu.edu/model/lc50.php).

Checkerboard interaction assays

Antibacterial activities of combinations of PUM and Rif were assessed in checkerboard interaction assays (White et al., 1996; Meletiadis et al., 2010; Figure 1E). Broth-macrodilution assays (procedures as in CLSI/NCCLS, 2009) were performed in checkerboard format, using *S. pyogenes* strain L49 or *S. pneumoniae* strain L44, and using Todd Hewitt broth (BD Biosciences) containing pairwise combinations of: (i) PUM at 1x, 0.5x, 0.25x, 0.125x, 0.063x, 0.031x, 0.016x, and 0.0078x MIC_{PUM} and (ii) Rif at 0.8x, 0.4x, 0.2x, 0.1x,

0.05x, 0.025x, and 0.0125x MIC_{Rif}. Fractional inhibitory concentrations (FICs), FIC indices (FICIs), and minimum and maximum FICIs ($FICI_{min}$ and $FICI_{max}$) were calculated as in Meletiadis et al., 2010. $FICI_{min} \leq 0.5$ was deemed indicative of super-additivity (synergism), $FICI_{min} > 0.5$ and $FICI_{max} \leq 4.0$ was deemed indicative of additivity, and $FICI_{max} > 4.0$ was deemed indicative of sub-additivity (antagonism) (White et al., 1996; Meletiadis et al., 2010).

Spontaneous resistance rate assays

Spontaneous resistance rates were determined in Luria-Delbrück fluctuation assays (Figure 2A; procedures as in Srivastava et al., 2012). *S. pyogenes* strain ATCC 12344 ($\sim 1 \times 10^9$ cfu/plate) was plated on Todd Hewitt agar [Todd Hewitt broth (BD Biosciences) supplemented with 1.5% Bacto agar (BD Biosciences)] containing 64 μg/mL or 128 μg/mL PUM (8x or 16x MIC under these conditions) or 1 μg/mL or 2 μg/mL Rif (8x or 16x MIC under these conditions), and numbers of colonies were counted after 24 hr at 37°C (at least six independent determinations each). Resistance rates and 95% confidence intervals were calculated using the Ma-Sandri-Sarkar Maximum Likelihood Estimator (Ma et al., 1992; Sarkar et al., 1992) as implemented on the Fluctuation Analysis Calculator (Hall et al., 2009; http://www.keshavsingh.org/protocols/FALCOR.html).

Spontaneous PUM-resistant mutants, *S. pyogenes*

To isolate spontaneous PUM-resistant mutants of *S. pyogenes* (Figure 2B), a single colony of *S. pyogenes* ATCC 12344 was inoculated into 5 mL Todd Hewitt broth (BD Biosciences) and incubated 3 hr at 37°C with shaking in a 7% CO_2/6% O_2/4% H_2/83% N_2 atmosphere (atmosphere controlled using Anoxomat AN2CTS; Advanced Instruments), the culture was centrifuged, and the cell pellet ($\sim 1 \times 10^9$ cells) was re-suspended in 50 μL Todd Hewitt broth and plated on Todd Hewitt agar (BD Biosciences) containing 16-256 μg/mL PUM (2-32x MIC under these conditions), and plates were incubated 120 hr at 37°C in a 7% CO_2/6% O_2/4% H_2/83% N_2 atmosphere. PUM-resistant mutants were identified by the ability to form colonies on these media, were confirmed to be PUM-resistant by re-streaking on the same media, and were confirmed to be *S. pyogenes* (as opposed to contaminants) using Taxo A differentiation discs (BD Biosciences) and Pyrase strips (Fluka/Sigma-Aldrich).

Genomic DNA was isolated using the Wizard Genomic DNA Purification Kit [Promega; procedures as specified by the manufacturer, but with cells lysed using 1 mg/mL lysozyme (Sigma-Aldrich)] and was quantified by measurement of UV-absorbance (procedures as in Sambrook and Russell, 2001). The *rpoC* gene and the *rpoB* gene were PCR-amplified in reactions containing 0.2 μg genomic DNA, 0.4 μM forward and reverse oligodeoxyribonucleotide primers (5′-GGGCAAATGATAACTTAGTTGCGATTTGCTG-3′ and 5′-CCTTTCTGCCTTTGATGACTTTACCAGTTC-3′ for *rpoB;* 5′-GCTCAAGAAACTCAAGAAGTTTCTGAAACAACTGAC-3′ and 5′-GTCAATGCTTTTTACTGCCAACAAACTCAGAC-3′ for *rpoC*), 5 U Taq DNA polymerase (Genscript), and 800 μM dNTP mix (200 μM each dNTP; Agilent/Stratagene) (initial denaturation step of 3 min at 94°C; 30 cycles of 30 s at 94°C, 45 s at 53°C, and 4 min at 68°C; final extension step of 10 min at 68°C). PCR products containing the *rpoC* gene (3.6 kB) or the *rpoB* gene (3.6 kB) were isolated by electrophoresis on 0.8% agarose gels (procedures as in Sambrook and Russell, 2001), extracted from gel slices using a Gel/PCR DNA Fragments Extraction Kit (IBI Scientific; procedures as specified by the manufacturer), and sequenced (GENEWIZ; Sanger sequencing; seven sequencing primers per gene).

Spontaneous PUM-resistant mutants, *E. coli*

To isolate spontaneous PUM-resistant mutants of *E. coli* (Figure S3A), *E. coli* uptake-proficient, efflux-deficient strain D21f2tolC (Fralick and Burns-Keliher, 1994) was cultured to saturation in 10 mL LB broth (Sambrook and Russell, 2001) at 37°C, cultures were centrifuged, cell pellets ($\sim 1 \times 10^{10}$ cells) were re-suspended in 50 μL LB broth and plated on LB agar (Sambrook and Russell, 2001) containing 800 μg/mL PUM (~1x MIC under these conditions), and plates were incubated 96-120 hr at 37°C. PUM-resistant mutants were identified by the ability to form colonies on this medium.

Genomic DNA was isolated, and *rpoB* and *rpoC* genes were PCR-amplified and sequenced, as in Degen et al., 2014.

Resistance and cross-resistance levels

Resistance levels of *S. pyogenes* and *E. coli* spontaneous PUM-resistant mutants (Figures 2B and S3B) were quantified in broth-microdilution assays. A single colony of a mutant strain or the isogenic wild-type parent strain was inoculated into 5 mL Todd Hewitt broth (BD Biosciences; for *S. pyogenes*) or LB broth (Sambrook and Russell, 2001; for *E. coli*) and incubated at 37°C with shaking in a 7% CO_2/6% O_2/4% H_2/83% N_2 atmosphere (atmosphere controlled using Anoxomat AN2CTS; Advanced Instruments); for *S. pyogenes*) or in air (for *E. coli*) until OD_{600} = 0.4-0.8. Diluted aliquots ($\sim 2 \times 10^5$ cells in 50 μL same medium) were dispensed into wells of a 96-well microplate containing 50 μL of the same medium or 50 μL of a 2-fold dilution series of PUM in the same medium (final PUM concentration = 0 or 0.098-800 μg/mL), and were incubated 16 hr at 37°C with shaking in a 7% CO_2/6% O_2/4% H_2/83% N_2 atmosphere (for *S. pyogenes*) or in air (for *E. coli*). MIC was defined as the lowest tested concentration of PUM that inhibited bacterial growth by ≥ 90%. $MIC/MIC_{wild\text{-}type}$ was defined as the ratio of MIC for mutant to MIC for isogenic wild-type parent (*S. pyogenes* $MIC_{wild\text{-}type}$ = 6.25 μg/mL under these conditions; *E. coli* $MIC_{wild\text{-}type}$ = 400 μg/mL under these conditions).

Cross-resistance levels of *S. pyogenes* and *E. coli* spontaneous PUM-resistant mutants (Figures 2E and S3F) were determined as in the preceding paragraph, but using culture aliquots ($\sim 1x10^5$ cells) in 97 μL growth medium supplemented with 3 μL methanol or 3 μL of a 2-fold dilution series of Rif (Sigma-Aldrich; *S. pyogenes* $MIC_{wild\text{-}type}$ = 0.098 μg/mL; *E. coli* $MIC_{wild\text{-}type}$ = 0.20 μg/mL), lipiarmycin A3 (Lpm; BioAustralis; *S. pyogenes* $MIC_{wild\text{-}type}$ = 6.25 μg/mL; *E. coli* $MIC_{wild\text{-}type}$ = 1.56 μg/mL), myxopyronin B (Myx;

prepared as in Ebright and Ebright, 2012; *S. pyogenes* $MIC_{wild\text{-}type}$ = 6.25 μg/mL; *E. coli* $MIC_{wild\text{-}type}$ = 0.20 μg/mL), streptolydigin (Stl; Sourcon-Padena; *S. pyogenes* $MIC_{wild\text{-}type}$ = 3.13 μg/mL; *E. coli* $MIC_{wild\text{-}type}$ = 3.13 μg/mL), CBR703 (CBR; Maybridge; *E. coli* $MIC_{wild\text{-}type}$ = 6.25 μg/mL), or salinamide A (Sal; gift of W. Fenical, Scripps Institution of Oceanography; *E. coli* $MIC_{wild\text{-}type}$ = 0.049 μg/mL) in methanol (final concentrations = 0 and 0.006-50 μg/mL), or using culture aliquots (~2x10^5 cells) in 50 μL growth medium supplemented with 50 μL growth medium or 50 μL of a 2-fold dilution series of GE23077 (GE; prepared as in Ciciliato et al., 2004; *E. coli* $MIC_{wild\text{-}type}$ = 500 μg/mL) in growth medium (final concentrations = 0 and 125-8000 μg/mL).

Cross-resistance levels of *S. pyogenes* Rif-resistant mutants to PUM (Figure 1E) were determined as described for cross-resistance levels of *S. pyogenes* spontaneous PUM-resistant mutants, but analyzing a collection of 13 *S. pyogenes* spontaneous Rif-resistant mutants [isolated and sequenced using the same procedures used for isolation and sequencing of *S. pyogenes* PUM-resistant mutants (Methods, Spontaneous PUM-resistant mutants, *S. pyogenes*), but using Todd Hewitt agar containing 1-16x MIC Rif (0.1-2 μg/mL under these conditions)] and the isogenic wild-type parent, and analyzing a 2-fold dilution series of PUM (final concentration = 0 or 1.56-100 μg/mL).

Cross-resistance levels of *E. coli* Rif-, Lpm-, Myx-, and Sal-resistant mutants to PUM (Figures S3G–S3I and S3L) were determined as described for resistance levels of *E. coli* spontaneous PUM-resistant mutants, but analyzing a collection of *E. coli* D21f2tolC derivatives comprising four chromosomal Rif-resistant mutants, five chromosomal Lpm-resistant mutants, five chromosomal Myx-resistant mutants, five chromosomal Sal-resistant mutants, and the isogenic wild-type parent (Degen et al., 2014), and analyzing a 2-fold dilution series of PUM (final concentration = 0 or 25-1600 μg/mL).

Cross-resistance levels of *E. coli* Stl-, CBR-, and GE-resistant mutants to PUM (Figures S3J, S3K, and S3N) were determined analogously, analyzing a collection of *E. coli* D21f2tolC pRL706 and *E. coli* D21f2tolC pRL663 derivatives comprising five plasmid-based Stl-resistant mutants, five plasmid-based CBR-resistant mutants, six plasmid-based GE-resistant mutants, and plasmid-based wild-type isogenic parents (Tuske et al., 2005; Zhang et al., 2014; Feng et al., 2015). Single colonies were inoculated into 5 mL LB broth containing 200 μg/mL ampicillin (Sigma-Aldrich), incubated at 37°C with shaking until OD_{600} = 0.4-0.8, supplemented with IPTG (Gold Bio) to a final concentration of 1 mM, and further incubated 1 hr at 37°C with shaking. Diluted aliquots (~2 × 10^5 cells in 50 μL LB broth containing 200 μg/mL ampicillin and 1 mM IPTG) were dispensed into wells of a 96-well microplate containing 50 μL of the same medium or 50 μL of a 2-fold dilution series of PUM in the same medium (final concentration = 0 or 25-4000 μg/mL), and were incubated 16 hr at 37°C with shaking.

Amino-acid substitutions that confer PUM-resistance in the context of *S. pyogenes* RNAP were re-constructed and re-analyzed in the context of *E. coli* RNAP using an *E. coli* plasmid-based resistance assay (Figure S3B). Site-directed mutagenesis (QuikChange Site-Directed Mutagenesis Kit; Agilent) was used to construct plasmid pRL706 (Severinov et al., 1997) and pRL663 (Wang et al., 1995) derivatives encoding *E. coli* RNAP β-subunit and β'-subunit derivatives having amino-acid substitutions that confer PUM-resistance in *S. pyogenes* (sequences from Figure 2B). The resulting plasmids were introduced by transformation into *E. coli* strain D21f2tolC (Fralick and Burns-Keliher, 1994), and resistance levels of transformants were determined using the procedures of the preceding paragraph.

Formation of RNAP-promoter open complex

Experiments (Figure S4A) were performed as in Mukhopadhyay et al., 2008. Reaction mixtures contained (20 μL): test compound (0 or 500 μM PUM, 2 μM Rif, or 100 μM Lpm), 40 nM *E. coli* RNAP σ^{70} holoenzyme, 10 nM Cy5-labeled DNA fragment carrying positions −40 to +15 of *lacUV5* promoter (*lacUV5*-[-40;+15]-Cy5; Mukhopadhyay et al., 2008), and 100 μg/mL heparin, in 50 mM Tris-HCl (pH 8.0), 100 mM KCl, 10 mM $MgCl_2$, 1 mM dithiothreitol, 10 μg/mL bovine serum albumin, and 5% glycerol. Reaction components other than DNA and heparin were incubated 10 min at 37°C; DNA was added and reactions were incubated 15 min at 37°C; and heparin was added and reactions were incubated 2 min at 37°C. Products were applied to 5% TBE-polyacrylamide slab gels (Bio-Rad), electrophoresed in TBE (Sambrook and Russell, 2001), and analyzed by fluorescence scanning (Typhoon 9400; GE Healthcare).

Nucleotide addition in transcription initiation

Experiments were performed as in Zhang et al., 2014, using reaction mixtures that contained no inhibitor, 500 μM PUM, 2 μM Rif, or 100 μM Lpm, and using 5 μM [α^{32}P]UTP (3 Bq/fmol; PerkinElmer) (Figure S4B).

Nucleotide addition in transcription elongation

Experiments were performed as in Zhang et al., 2014, using reaction mixtures that contained no inhibitor, 500 μM PUM, 2 μM Rif, or 100 μM Lpm (Figure S4C).

Nucleotide addition at elevated NTP concentrations

Experiments (Figure 3A) were performed as described above for assays of promoter-dependent transcription by *B. subtilis* RNAP (Methods, RNAP-inhibitory activity in vitro), using reaction mixtures (50 μL) that contained 0 or 6 μM PUM, 0.4 U *E. coli* RNAP σ^{70} holoenzyme (Epicentre), 0.4 nM plasmid pUC19 (Clontech/Takara), 80 mM HEPES-KOH (pH 7.6), 80 mM KCl, 4 mM $MgCl_2$, 0.1 mM EDTA, 5 mM dithiothreitol, 100 μg/mL bovine serum albumin, and either (i) 100 μM ATP, 100 μM [α^{32}P]CTP (0.2 Bq/fmol; PerkinElmer), 100 μM GTP, and 10-500 μM UTP; (ii) 10-500 μM GTP, 100 μM ATP, 100 μM CTP, and 2 μM [α^{32}P]UTP (0.2 Bq/fmol; PerkinElmer); (iii) 100 μM GTP, 10-500 μM ATP, 100 μM CTP, and 2 μM [α^{32}P]UTP (0.2 Bq/fmol); or (iv) 100 μM GTP,

100 μM ATP, 10-500 μM CTP, and 2 μM [α^{32}P]UTP (0.2 Bq/fmol). The reaction time was 30 min at 37°C. Relative nucleotide incorporation was defined as the ratio of nucleotide incorporation in the presence of PUM to nucleotide incorporation in the absence of PUM.

Nucleotide addition on standard and "U-less cassette" templates

Experiments (Figure 3B) were performed as described in the preceding section (Methods, Nucleotide addition at elevated NTP concentrations), using reaction mixtures (50 μL) that contained 0-20 μM PUM, 0.4 U *E. coli* RNAP σ^{70} holoenzyme (Epicentre), 2 μM [α^{32}P]CTP (0.2 Bq/fmol; PerkinElmer), 100 μM ATP, 100 μM GTP, and 5 μM UTP, in 40 mM Tris-HCl (pH 7.5), 10 mM $MgCl_2$, 5 mM dithiothreitol, 15 mM KCl, 0.01% Triton X-100, and 100 μg/mL bovine serum albumin, and either (i) 50 nM DNA fragment carrying positions −112 to +8 of the *E. coli recA* promoter (Sancar et al., 1980) followed by 5′-CAGGGACAAGTTAGTTCGTTCAGCGACACGCGGCAACAAG-3′ (directs incorporation of U, G, A, and C) or (ii) 50 nM DNA fragment carrying positions −112 to +8 of the *E. coli recA* promoter followed by 5′-CAGGGACAAGGAGACCAACGCAGCGACACGCGGCAACAAG-3′ ("U-less cassette"; directs incorporation of G, A, and C). The reaction time was 60 min at 37°C. Relative nucleotide incorporation was defined as the ratio of nucleotide incorporation in the presence of PUM to nucleotide incorporation in the absence of PUM.

Template-sequence specificity of inhibition by PUM: single-nucleotide-addition reactions

Template-sequence specificity of inhibition by PUM was assessed in single-nucleotide-addition experiments (Figure 3C) using *E. coli* RNAP transcription elongation complexes assembled on the nucleic-acid scaffolds in Table S5.

Nucleic-acid scaffolds for single-nucleotide-addition reactions were prepared as follows: 1 μM nontemplate-strand oligodeoxyribonucleotide [5′-ACGCCAGACAGGG-3′ or 5′-TCGCCAGACAGGG-3′; IDT], 1 μM template-strand oligodeoxyribonucleotide [3′-GCCGCGCG-(C or T or A or G)-(A or C or G)-TGCGGTCTGTCCC-5′ or 3′-GCCGCGCG-(C or T or A or G)-(T)-AGCGGTCTGTCCC-5′; IDT], and 1 μM ^{32}P-5′ end-labeled oligoribonucleotide [5′-^{32}P-CGGCGCGC-(U or C or A or G)-3′; 90 Bq/fmol; prepared using T4 polynucleotide kinase (New England Biolabs), [γ^{32}P]ATP (100 Bq/fmol; PerkinElmer), and corresponding unlabelled oligoribonucleotide (IDT); procedures as in Sambrook and Russell, 2001], in 5 mM Tris-HCl (pH 7.7), 200 mM NaCl, and 10 mM $MgCl_2$, were heated 5 min at 95°C, cooled to 4°C in 2°C steps with 1 min/step using a thermal cycler (Applied Biosystems), and stored at −20°C. Reaction mixtures for single-nucleotide-addition reactions contained (10 μL): 0 or 25 μM PUM, 40 nM *E. coli* RNAP core enzyme, 10 nM nucleic-acid scaffold, and 2.5 μM ATP, GTP, CTP, or UTP, in 50 mM Tris-HCl (pH 8.0), 100 mM KCl, 10 mM $MgCl_2$, 1 mM dithiothreitol, 10 μg/mL BSA, and 5% glycerol. Reaction components except PUM and NTP were pre-incubated 10 min at 37°C, PUM was added and reaction mixtures were incubated 5 min at 37°C, and NTP was added and reaction mixtures were incubated 5 min at 37°C. Reactions were terminated by addition of 5 μL 80% formamide, 10 mM EDTA, 0.04% bromophenol blue, 0.04% xylene cyanol, and 0.08% amaranth red, and heating 2 min at 95°C. Samples were applied to denaturing 15% polyacrylamide (19:1 acrylamide:bisacrylamide; 7 M urea) slab gels (Sambrook and Russell, 2001), electrophoresed in TBE (Sambrook and Russell, 2001), and analyzed by storage-phosphor scanning (Typhoon 9400; GE Healthcare).

Template-sequence specificity of inhibition by PUM: multiple-nucleotide-addition reactions

Template-sequence specificity of inhibition by PUM was assessed in multiple-nucleotide-addition experiments (Figure 3D), performed by adding PUM to transcription elongation complexes halted at position +29 of a 100 bp transcription unit by omission of CTP, re-starting transcription elongation complexes and allowing transcription of positions +30 to +100 of the transcription unit by addition of CTP, and identifying positions at which PUM inhibits transcription.

Halted transcription elongation complexes were prepared as in Revyakin et al., 2006. Reaction mixtures (20 μL) contained: 40 nM *E. coli* RNAP σ^{70} holoenzyme, 10 nM DNA fragment N25-100-tR2 (Revyakin et al., 2006), 100 μg/mL heparin, 5 μM [γ^{32}P]ATP (6 Bq/fmol; PerkinElmer), 5 μM UTP, and 5 μM GTP, in 50 mM Tris-HCl (pH 8.0), 100 mM KCl, 10 mM $MgCl_2$, 1 mM dithiothreitol, 10 μg/mL bovine serum albumin, and 5% glycerol. Reaction components other than heparin and NTPs were pre-incubated 5 min at 30°C; heparin was added and reaction mixtures were incubated 2 min at 30°C; NTPs were added and reaction mixtures were incubated 3 min at 30°C. Halted transcription elongation complexes were provided with PUM (1.25 μL 125 μM PUM, 1.25 μL 250 μM PUM, 1.25 μL 500 μM PUM, or 1.25 μL 1 mM PUM) or, to provide markers, chain-terminating 3′-O-methyl-NTPs (RiboMed; 1.25 μL 400 μM 3′-O-methyl-UTP, 1.25 μL 400 μM 3′-O-methyl-CTP, 1.25 μL 400 μM 3′-O-methyl-GTP, or 1.25 μL 400 μM 3′-O-methyl-ATP), were incubated 3 min at 30°C, were re-started by addition of 0.625 μL 200 μM UTP, 1.25 μL 200 μM CTP, 0.625 μL 200 μM GTP, and 0.625 μL 200 μM ATP, and were further incubated 10 min at 30°C. Reactions were terminated by addition of 12.5 μL 80% formamide, 10 mM EDTA, 0.04% bromophenol blue, 0.04% xylene cyanol, and 0.08% amaranth red, and heating 4 min at 95°C. Samples were applied to denaturing 10% polyacrylamide (19:1 acrylamide:bisacrylamide; 7 M urea) slab gels (Sambrook and Russell, 2001), electrophoresed in TBE (Sambrook and Russell, 2001), and analyzed by storage-phosphor scanning (Typhoon 9400; GE Healthcare).

Structure determination: RPo-GpA-PUM

Crystals of *T. thermophilus* RPo-GpA were prepared as in Zhang et al., 2012. Crystallization drops contained 1 μL 18 μM RPo (prepared from *T. thermophilus* RNAP σ^{A} holoenzyme and synthetic nucleic-acid scaffold as in Zhang et al., 2012) and 1 mM GpA (TriLink) in 20 mM Tris-HCl, pH 7.7, 100 mM NaCl, and 1% glycerol, and 1 μL reservoir buffer (RB; 100 mM Tris-HCl, pH 8.4, 200 mM KCl,

50 mM $MgCl_2$, and 10% PEG4000), and were equilibrated against 400 μL RB in a vapor-diffusion hanging-drop tray (Hampton Research). Rod-like crystals appeared in 1 day, and grew to a final size of 0.1 mm x 0.1 mm x 0.3 mm in 5 days.

PUM was soaked into RPo-GpA crystals by adding 0.2 μL 100 mM PUM in RB to the crystallization drop and incubating 30 min at 22°C. RPo-GpA-PUM crystals were transferred to reservoir solutions containing 2 mM PUM in 17.5% (v/v) (2R,3R)-(-)-2,3-butanediol (Sigma-Aldrich) and were flash-cooled with liquid nitrogen.

Diffraction data for RPo-GpA-PUM were collected from cryo-cooled crystals at Cornell High Energy Synchrotron Source (CHESS) beamline F1. Data were integrated and scaled using HKL2000 (Otwinowski and Minor, 1997). Structure factors were converted using the French-Wilson algorithm (French and Wilson, 1978) in Phenix (Adams et al., 2010) and were subjected to anisotropy correction using the UCLA MBI Diffraction Anisotropy server (Strong et al., 2006; http://services.mbi.ucla.edu/anisoscale/). The structure of RPo-GpA-PUM was solved by molecular replacement in Molrep (Vagin and Teplyakov, 1997), using one RNAP molecule from the structure of *T. thermophilus* RPo (PDB 4G7H; Zhang et al., 2012) as the search model. Early-stage refinement included rigid-body refinement of each RNAP molecule, followed by rigid-body refinement of each subunit of each RNAP molecule. Cycles of iterative model building with Coot (Emsley et al., 2010) and refinement with Phenix (Adams et al., 2010) were performed. Atomic models of the DNA nontemplate strand, the DNA template strand, and GpA were built into the mFo-DFc omit map, and further refinement with Phenix was performed. The atomic model of PUM was built into the mFo-DFc omit map and was refined with Phenix. The final crystallographic model of RPo-GpA-PUM at 3.30 Å resolution, refined to Rwork and Rfree of 0.232 and 0.280, has been deposited in the PDB with accession code PDB: 5X21 (Figure 4A; Table S3).

Structure determination: RPo-GpA-CMPcPP

Crystals of *T. thermophilus* RPo-GpA-CMPcPP were prepared by co-crystallization. Crystallization drops contained 1 μL 18 μM RPo (prepared from *T. thermophilus* RNAP σ^A holoenzyme and synthetic nucleic-acid scaffold as in Zhang et al., 2012), 1 mM GpA (TriLink), and 10 mM CMPcPP (Jena Bioscience) in 20 mM Tris-HCl, pH 7.7, 100 mM NaCl, and 1% glycerol, and 1 μL RB, and were equilibrated against 400 μL RB in a vapor-diffusion hanging-drop tray (Hampton Research). Rod-like crystals appeared in 1 day, and grew to a final size of 0.1 mm x 0.1 mm x 0.3 mm in 5 days. RPo-GpA-CMPcPP crystals were transferred to reservoir solutions containing 2 mM CMPcPP in 17.5% (v/v) (2R,3R)-(-)-2,3-butanediol (Sigma-Aldrich), and were flash-cooled with liquid nitrogen.

Diffraction data for RPo-GpA-CMPcPP were collected from cryo-cooled crystals at CHESS beamline F1. Data were integrated and scaled, structure factors were converted and subjected to anisotropy correction, and the structure was solved and refined using procedures analogous to those in the preceding section. The final crystallographic model of RPo-GpA-CMPcPP at 3.35 Å resolution, refined to Rwork and Rfree of 0.208 and 0.250, has been deposited in the PDB with accession code PDB: 5X22 (Figure 4B; Table S3).

Semi-synthesis of PUM derivatives

Semi-syntheses of PUM derivatives from PUM corroborate the inferred structure of PUM, provide routes for preparation of novel PUM derivatives, and provide initial structure-activity relationships (Figures 5A, 5C, and 5D). Reactions were conducted starting from 1 mg PUM, and products were identified by LC-MS (Agilent 1100 with flow split in 1:1 ratio between UV detector and ion-trap ESI-MS interface of Bruker Esquire 3000 Plus; Waters Atlantis 3 μm, 50 × 4.6 mm, column; phase A = 0.05% trifluoroacetic acid in water; phase B = acetonitrile; gradient = 5%–95% B in 6 min; flow rate = 1 mL/min; run temperature = 40°C; PUM retention time = 1.4 min).

Reaction of PUM with $TiCl_3$ in 1 M sodium acetate (pH 7.0) for 2 hr at room temperature resulted in reduction of the N-hydroxy moiety, yielding desoxy-PUM (**1**; *m/z* = 471 $[M+H]^+$). Reaction of PUM with $PdCl_2$ (Maffioli et al., 2005) in 1:1 acetonitrile:water for 2 hr at room temperature resulted in selective dehydration of the PUM glutamine sidechain amide, yielding nitrile analog **2** (*m/z* = 469 $[M+H]^+$). Reaction of PUM with 0.1% TFA in water for 3 days at room temperature resulted in hydrolysis of the glutamine side-chain amide, yielding carboxy analog **3** (*m/z* = 488 $[M+H]^+$). Reaction of **3** with benzylamine in DMF containing benzotriazol-1-yl-oxy-tripyrrolidinophosphonium hexafluorophosphate (PyBOP) for 30 min at room temperature yielded benzylamide analog **4** (*m/z* = 577 $[M+H]^+$). Reaction of PUM with 2,3-butanedione (Leitner and Lindner, 2003) in 10 mM ammonium acetate (pH 8.0) for 30 min at room temperature resulted in diolic intermediate **5** (*m/z* = 573 $[M+H]^+$), which subsequently was trapped by treatment with phenylboronic acid for 2 hr at room temperature, yielding phenyl-dioxaborolan analog **6** (*m/z* = 659 $[M+H]^+$).

Total synthesis of desoxy-PUM

Total synthesis of desoxy-PUM provides a reference compound that corroborates the inferred stereochemistry of PUM [by comparison of desoxy-PUM prepared by total synthesis (**1** in Figure 5B) to desoxy-PUM prepared by semi-synthesis from PUM (**1** in Figure 5A)] and provides an additional route to novel PUM derivatives. Desoxy-PUM was obtained in eight steps by convergent synthesis from commercially available β-D-pseudouridine and glycyl-L-glutamine, as follows (Figure 5B).

Acetonide protection

Reaction a in Figure 5B. To a solution of β-D-pseudouridine (Berry & Associates; 400 mg, 1.64 mmol) and 2,2-dimethoxypropane (Sigma-Aldrich; 12 mL) in dimethylformamide (8 mL), concentrated HCl (80 μL) was added, and the reaction mixture was stirred

5 hr at room temperature. After neutralization with 2.5 M NaOH, solvent was removed under vacuum. ^{1}H-NMR (400 MHz, D_2O, δ-H): 1.35 (s, 3H, CH_3), 1.56 (s, 3H, CH_3), 3.67 (dd, 1H, J = 12.2, 5.65 Hz, H-5′), 3.75 (dd, 1H, J = 12.2, 3.75 Hz, H-5′), 4.11 (dd, 1H, H-4'), 4.75 (m, 2H), 4.86 (m, 1H), 7.62 (s, 1H, H-6).

Mesylation

Reaction b in Figure 5B. To a solution of the crude product of the preceding step (419 mg, 1.47 mmol) in pyridine (Sigma-Aldrich; 4.7 mL), methanesulfonyl chloride (Sigma-Aldrich: 95 μL, 1.23 mmol) was added with stirring at 0°C. The reaction mixture was stirred at room temperature until completeness (16 h). Solvent was removed by rotary evaporation, and the raw material was purified by flash chromatography on Combiflash (Teledyne ISCO), yielding 475 mg of a white powder (95% yield). ^{1}H-NMR (400 MHz, acetonitrile-d_3, δ-H): 1.32 (s, 3H, CH_3), 1.54 (s, 3H, CH_3), 4.33 (dd, 1H, J = 11 Hz, H-5′), 4.46 (dd, 1H, J = 11 Hz, H-5′), 4.20 (m, 1H), 4.72 (dd, 1H), 4.80 (m, 2H), 7.55 (s, 1H, H-6), 10.23 (sb, 1H, NH), 10.45 (sb, 1H, NH).

Azidation

Reaction c in Figure 5B. To a solution of the product of the preceding step (475 mg) in dimethylformamide (24 mL), sodium azide (Sigma-Aldrich: 476 mg) was added, the reaction mixture was stirred 4 hr at 100°C, and solvent was removed by rotary evaporation. ^{1}H-NMR (400 MHz, acetonitrile-d_3, δ-H): 1.30 (s, 3H, CH_3), 1.50 (s, 3H, CH_3), 3.52 (d, 2H, J = 5.3 Hz, H-5′), 4.04 (m, 1H, H-3′), 4.69 (dd, 1H, H-4'), 4.75 (d, 1H, J = 3.3 Hz, H-1'), 4.87 (dd, 1H, J = 3.3 Hz, H-2′), 7.58 (s, 1H, H-6).

Azide reduction

Reaction d in Figure 5B. To a solution of the crude product of the preceding step (193 mg) in tetrahydrofuran (8.8 mL) and water (1.8 mL), 1 M trimethylphosphine in tetrahydrofuran (Sigma-Aldrich; 0.74 mL) was added, the reaction mixture was stirred 2 hr at room temperature, and solvent was removed by rotary evaporation. ^{1}H-NMR (400 MHz, D_2O, δ-H): 1.47 (s, 3H, CH_3), 168 (s, 3H, CH_3), 3.40 (dd, 1H, H-5′), 3.49 (dd, 1H, H-5′),4.38 (m, 1H, H-4'), 4.90 (dd, 1H, H-1'), 4.94 (d, 1H, H-3′), 5.05 (dd, 1H, H-2′), 7.76 (s, 1H, H-6).

Fmoc protection

Reaction e in Figure 5B. To a solution of the crude product of the preceding step (22 mg, 0.11 mmol) in dioxane (150 μL) and water (250 μL) sodium carbonate (26.5 mg) was added, followed by Fmoc chloride (Sigma-Aldrich; 31 mg, 1.3 eq), and the reaction mixture stirred overnight at room temperature. After addition of water (5 mL), the reaction was extracted with ethyl acetate (3 × 5 mL), the combined organic extracts were extracted with saturated sodium bicarbonate (3 × 5 mL), the combined aqueous extracts were acidified to pH 1 with 1 M HCl and extracted with ethyl acetate (3 × 5 mL), and the combined organic extracts were treated with sodium sulfate and evaporated to dryness, providing Fmoc-glycl-L-glutamine in quantitative yield. ^{1}H-NMR (400 MHz, D_2O, δ-H): 1.98 (m, 1H, Asn-β), 2.18 (m, 1H, Asn-β), 2.33 (m, 2H, Asn-γ), 3.90 (m, 2H, Gly-α), 4.23 (m, 1H), 4.31 (m, 1H), 4.47 (dd, 1H, Asn-α), 7.31 (m, 2H, Ar), 7.38 (m, 2H, Ar), 7.69 (m, 2H, Ar), 7.81 (m, 2H, Ar).

Coupling, Fmoc deprotection, and formamidinylation

Reactions f-h in Figure 5B. To a solution of the product of the preceding step (20 mg) and the product of the azide-reduction reaction (30 mg, 1.1 eq) in dry dimethylformamide (1.5 mL), N,N′-dicyclohexylcarbodiimide (Sigma-Aldrich; 18 mg, 1.2 eq) and 1-hydroxybenzotriazole (Sigma-Aldrich; 19.5 mg, 2 eq) were added, and the reaction mixture was stirred overnight at room temperature, and the solvent was evaporated under reduced pressure. To a solution of the crude coupled product (12 mg) in dimethylformamide (800 μL), piperidine (200 μL) was added, and the reaction mixture was stirred 10 min at 25°C, the solvent was evaporated under reduced pressure, and the residue was washed with methylene chloride (2 × 5 mL). To a solution of the crude Fmoc-deprotected product (22 mg) in methanol (300 μL), 3,5-dimethylpyrazole-1-carboxamidine (Sigma-Aldrich; 45 mg, 10 eq) was added, and the reaction mixture was stirred overnight at room temperature, followed by 6 hr under reflux at 65°C to complete the reaction. The solvent was evaporated under reduced pressure, and the solid residue was washed with methylene chloride (2 × 10 mL). ^{1}H-NMR (400 MHz, D_2O/CD_3OD, δ-H): 1.33 (s, 3H, CH_3), 1.54 (s, 3H, CH_3), 2.01 (m, 1H, Asn-β), 2.17 (m, 1H, Asn-β), 2.37 (m, 2H, Asn-γ), 3.37 (m, 1H, H-5′), 3.65 (m, 1H, H-5′), 4.04 (s, 2H, Gly-α), 4.03 (m, 1H), 4.11 (m, 1H), 4.42 (m, 1H), 4.63 (m, 1H), 7.53 (s, 1H, H-6).

Acetonide deprotection

Reaction i in Figure 5B. A solution of the crude product of the preceding step (17 mg) in acetic acid:water (7:3; 2 mL) was stirred overnight at room temperature and then heated to 50°C for 10 hr under argon. The solvent was evaporated under reduced pressure, and the solid residue was washed with methylene chloride (2 × 5 mL) and methanol (2 mL), yielding a white solid that, when analyzed by LC-MS [performed as described for LC-MS of PUM (Methods, Structure Elucidation of PUM); retention time = 14 min], 1D- and 2D-NMR, was indistinguishable from desoxy-PUM obtained by reduction of PUM with $TiCl_3$ (**1** in Figure 5A). ^{1}H-NMR (600 MHz, DMSO-d_6 /D_2O, δ-H): 1.75 (m, 1H, Asn-β), 1.90 (m, 1H, Asn-β), 2.10 (m, 2H, Asn-γ), 3.29 (m, 2H, H-5′), 3.72 (m, 2H), 3.87 (s broad, 2H, Gly-α), 3.96 (m, 1H, H-2′), 4.24 (m, 1H, Asn-α), 4.40 (d, 1H, J = 5.3 Hz, H-1'), 6.73 (s broad, $CONH_2$), 7.32 (s broad, $CONH_2$), 7.40 (s, 1H), 8.11 (t broad, 1H, NH), 8.34 (d broad, 1H, NH-Asn). ^{13}C-NMR (DMSO-d_6, δ-H): 28.4, 31.9, 41.4, 44.0, 53.0, 72.3, 73.7, 79.9, 81.6, 110.4, 141.5, 152.2, 158.2, 164.2, 168.0, 171.3, 173.7.

QUANTITATION AND STATISTICAL ANALYSIS

Data for RNAP-inhibitory activities, growth-inhibitory activities, resistance, and cross-resistance are means of at least two technical replicates. Data for mouse infection models, resistance-rate assays, and checkerboard interaction assays are means and 95% confidence intervals for eight biological replicates, at least six biological replicates, and at least five technical replicates, respectively.

DATA AVAILABILITY

Atomic coordinates and structure factors for crystal structures of RPo-GpA-PUM and RPo-GpA-CMPcPP have been deposited in the Protein Data Bank with accession numbers PDB: 5X21 and 5X22. 16S rRNA gene sequences of PUM producer strains ID38640 and ID38673 have been deposited in GenBank with accession numbers GI: JQ929050 and JQ929051. PUM producer strain ID38640 has been deposited in the Deutsche Sammlung von Mikroorganismen und Zellkulturen patent depository collection with accession number DSMZ: DSM-26212. Both PUM producer strains, ID38640 and ID38673, can be obtained from NAICONS under a Material Transfer Agreement.

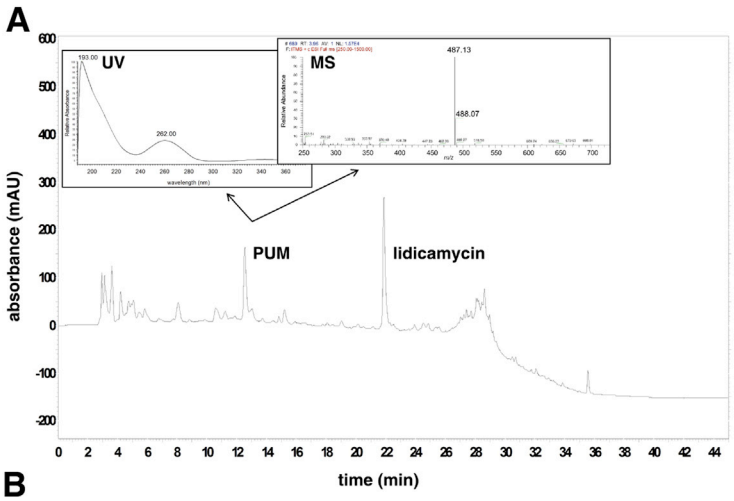

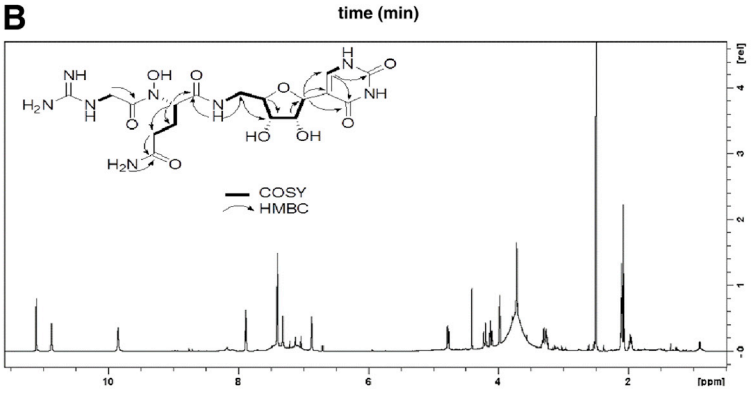

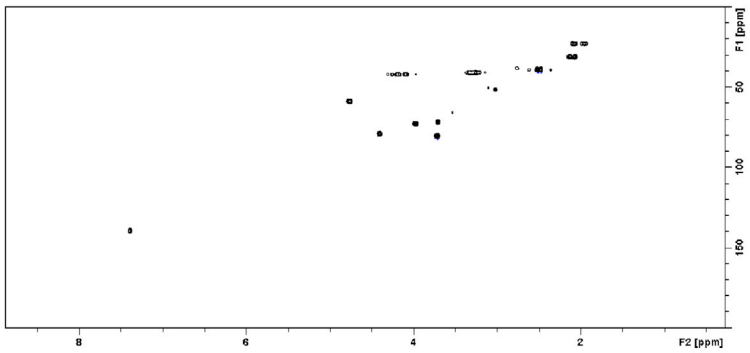

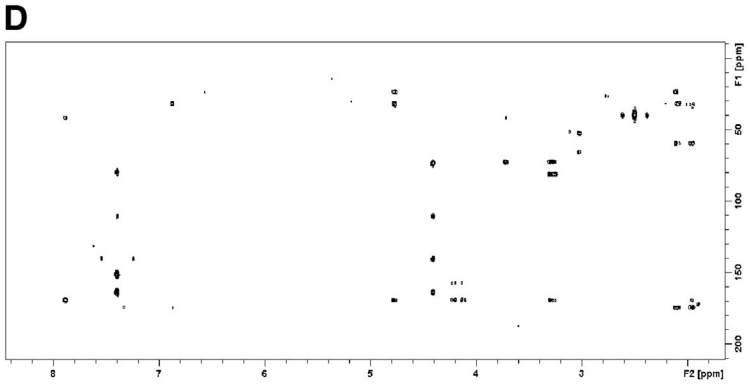

E

^{1}H-, ^{13}C-, and ^{15}N-NMR data of PUM in DMSO-d_6 at 25°C

		^{1}H (δ, ppm), multiplicity (J [Hz])	^{13}C (δ, ppm)	^{15}N (δ, ppm)
ribose	1'	4.34, d (4.70)	79.8	
	2'	3.91, dd (4.70, 5.32)	73.8	
	3'	3.65, m	76.3	
	4'	3.65, m	81.4	
	5'	3.24, m; 3.14, m	42	
	6'	7.82, t (5.62)		108.5
pseudouridine	1		110.7	
	2		164	
	3	11.04, d (1.92)		158.5
	4		152	
	5	10.8, dd (1.64)		131
	6	7.33, d (1.62)	140.4	
Gln	C=O		169.5	
	α	4.72, m	59	
	β	2.03, m; 1.90, m	23.6	
	γ	2.04, m; 1.91, m	31.7	
	δ		174	
	Nε	7.26, bs; 6.81, bs		108.9
Gly	NH	7.43, dd (4.95, 5.06)		75.1
	C=O		157	
	α	4.22, m; 4.12, m	43	

(legend on next page)

Figure S1. Isolation and Structure Elucidation of PUM, Related to Figure 1

(A) Chromatographic profile of *Streptomyces* sp. ID38640 culture extract, showing peaks for PUM and the unrelated metabolite lidicamycin, and UV-absorbance and mass spectra for PUM.

(B) Structure and ^{1}H-NMR spectrum of PUM in DMSO-d_6 at 25°C at 400 MHz.

(C) 2D-HSQC spectrum of PUM in DMSO-d_6 at 25°C at 400 MHz.

(D) 2D-HMBC spectrum of PUM in DMSO-d_6 at 25°C at 400 MHz.

(E) Summary of ^{1}H-, ^{13}C-, and ^{15}N-NMR data for PUM in DMSO-d_6.

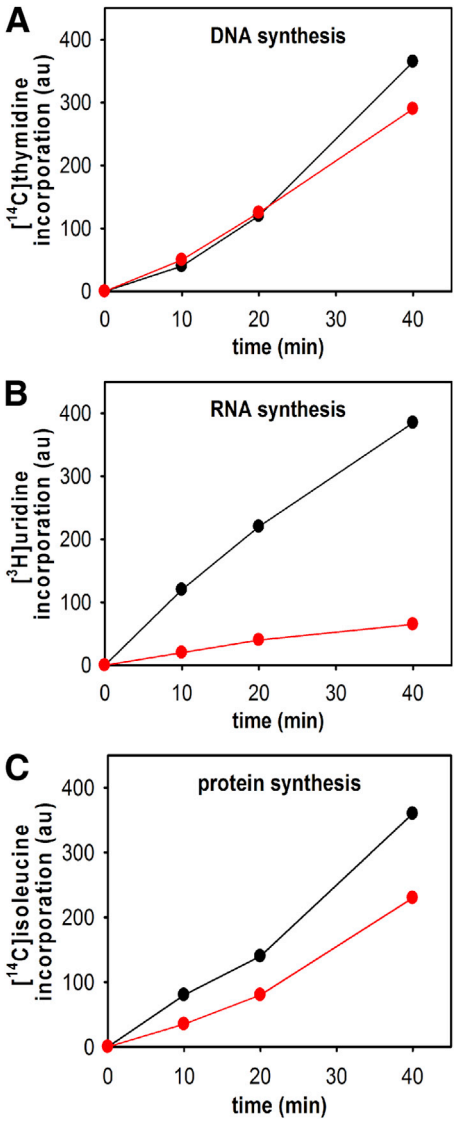

Figure S2. Effects of PUM on Macromolecular Synthesis in Bacterial Cells in Culture: Inhibition of RNAP-Dependent RNA Synthesis, Related to Figure 1

(A–C) Effects of PUM on DNA synthesis ([A]; [^{14}C]-thymidine incorporation), RNA synthesis ([B]; [^{3}H]-uridine incorporation), and protein synthesis ([C]; [^{14}C]-isoleucine incorporation) in *Staphylococcus simulans* in culture. Results match characteristic pattern for inhibition of RNAP-dependent RNA-synthesis (Degen et al., 2014; Lancini and Sartori, 1968; Lancini et al., 1969; Sergio et al., 1975; Irschik et al., 1983, 1985, 1995; Degen et al., 2014): i.e., rapid and strong inhibition of RNA synthesis, slower and weaker inhibition of protein synthesis, and little or no inhibition of DNA synthesis.

A

***E. coli* PUM-resistant mutants: sequences and properties**

amino acid substitution	number of independent isolates	resistance level (MIC/MIC$_{wild\text{-}type}$)
rpoB **(RNAP β subunit)**		
565 Glu→Asp	1	>16
565 Glu→Gly	1	>16

B

***E. coli* plasmid-based resistance assay**

amino acid substitution	resistance level (MIC/MIC$_{wild\text{-}type}$)
rpoB **(RNAP β subunit)**	
565 Glu→Gly	>4
565 Glu→Val	2
681 Met→Lys	>4
684 Asn→Ile	2
rpoC **(RNAP β′ subunit)**	
786 Thr→Arg	1
786 Thr→Lys	1
786 Thr→Met	2

C

***E. coli* PUM-resistant RNAP: *in vitro* resistance to PUM**

RNAP	resistance level (IC50/IC50$_{wild\text{-}type}$)
[565 Glu →Asp]β-RNAP	>150

D

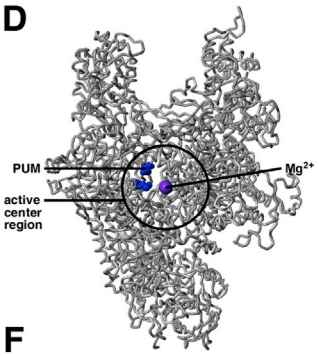

E

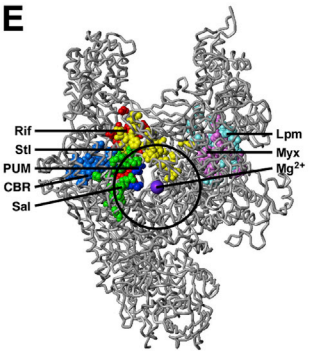

F

***E. coli* PUM-resistant mutants: cross-resistance to Rif, Stl, Myx, Lpm, CBR703, Sal, and GE**

amino acid substitution	resistance level (MIC/MIC$_{wild\text{-}type}$)						
	Rif	Lpm	Myx	Stl	CBR	Sal	GE
rpoB **(RNAP β subunit)**							
565 Glu→Asp	1	2	1	0.5	1	1	>16
565 Glu→Gly	1	0.25	1	0.5	2	2	>16

G

***E. coli* Rif-resistant mutants: absence of cross-resistance to PUM**

amino acid substitution	resistance level (MIC/MIC$_{wild\text{-}type}$)	
	Rif	PUM
rpoB **(RNAP β subunit)**		
516 Asp→Val	512	2
526 His→Asp	>1024	1
526 His→Tyr	>1024	0.5
531 Ser→Leu	1024	1

H

***E. coli* Lpm-resistant mutants: absence of cross-resistance to PUM**

amino acid substitution	resistance level (MIC/MIC$_{wild\text{-}type}$)	
	Lpm	PUM
rpoB **(RNAP β subunit)**		
1251 Tyr→Phe	8	1
1256 Gln→Glu	8	1
1256 Gln→Leu	8	1
rpoC **(RNAP β′ subunit)**		
337 Arg→His	8	1
337 Arg→Ser	8	2

I

***E. coli* Myx-resistant mutants: absence of cross-resistance to PUM**

amino acid substitution	resistance level (MIC/MIC$_{wild\text{-}type}$)	
	Myx	PUM
rpoB **(RNAP β subunit)**		
1275 Val→Met	128	1
1291 Leu→Phe	128	1
rpoC **(RNAP β′ subunit)**		
345 Lys→Arg	128	1
345 Lys→Asn	256	1
1354 Gly→Ser	16	2

J

***E. coli* Stl-resistant mutants: absence of cross-resistance to PUM**

amino acid substitution	resistance level (MIC/MIC$_{wild\text{-}type}$)	
	Stl	PUM
rpoB **(RNAP β subunit)**		
543 Ala→Val	64	1
545 Phe→Cys	>64	0.5
rpoC **(RNAP β′ subunit)**		
788 Leu→Met	32	0.25
1139 Pro→Arg	8	1
1139 Pro→Leu	8	1

K

***E. coli* CBR-resistant mutants: absence of cross-resistance to PUM**

amino acid substitution	resistance level (MIC/MIC$_{wild\text{-}type}$)	
	CBR	PUM
rpoB **(RNAP β subunit)**		
552 Pro→Met	4	1
618 Gln→Leu	4	0.5
642 Ser →Phe	4	1
654 Asp→His	4	1
657 Thr→Ile	4	1

L

***E. coli* Sal-resistant mutants: absence of cross-resistance to PUM**

amino acid substitution	resistance level (MIC/MIC$_{wild\text{-}type}$)	
	Sal	PUM
rpoB **(RNAP β subunit)**		
675 Asp→Ala	>256	2
677 Asn→Lys	>256	2
rpoC **(RNAP β′ subunit)**		
738 Arg→Pro	128	1
779 Ala→Val	256	1
782 Gly→Ala	>256	0.25

M

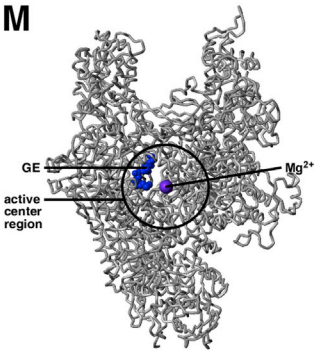

N

***E. coli* GE-resistant mutants: partial cross-resistance to PUM**

amino acid substitution	resistance level (MIC/MIC$_{wild\text{-}type}$)	
	GE	PUM
rpoB **(RNAP β subunit)**		
565 Glu→Asp	>16	10
566 Gly→Arg	16	1
566 Gly→Cys	8	1
566 Gly→Ser	4	1
684 Asn→Lys	>16	2
684 Asn→Thr	4	1

Figure S3. Target of PUM: RNAP NTP Addition Site: Results for Gram-Negative Bacterium *E. coli*, Related to Figure 2

(A) *E. coli* spontaneous PUM-resistant mutants.

(B) Effects of *S. pyogenes* PUM-resistant mutants (sequences from Figure 2B) when analyzed in *E. coli* plasmid-based resistance assay. Two substitutions confer moderate or higher (≥4x) resistance in *E. coli* plasmid-based resistance assay: β565 Glu→Gly and β681 Met→Lys.

(C) PUM-resistant phenotype of purified *E. coli* RNAP derivative containing β565 Glu→Asp substitution.

(D) Location of *E. coli* PUM target (sequences from [A] and [B] in three-dimensional structure of bacterial RNAP (colors as in Figure 2C).

(E) Absence of overlap between PUM target (blue) and Rif (red), Lpm (cyan), Myx (pink), Stl (yellow), CBR (light blue), and Sal (green) targets.

(F) Absence of cross-resistance of *E. coli* PUM-resistant mutants (sequences from [A]) to Rif, Lpm, Myx, Stl, CBR, and Sal.

(G–L) Absence of cross-resistance of *E. coli* Rif-, Lpm-, Myx-, Stl-, CBR-, and Sal-resistant mutants to PUM.

(M) Location of GE target (blue) in structure of bacterial RNAP. PUM target (D) shows partial overlap with GE target (M).

(N) Partial cross-resistance of *E. coli* GE-resistant mutants to PUM.

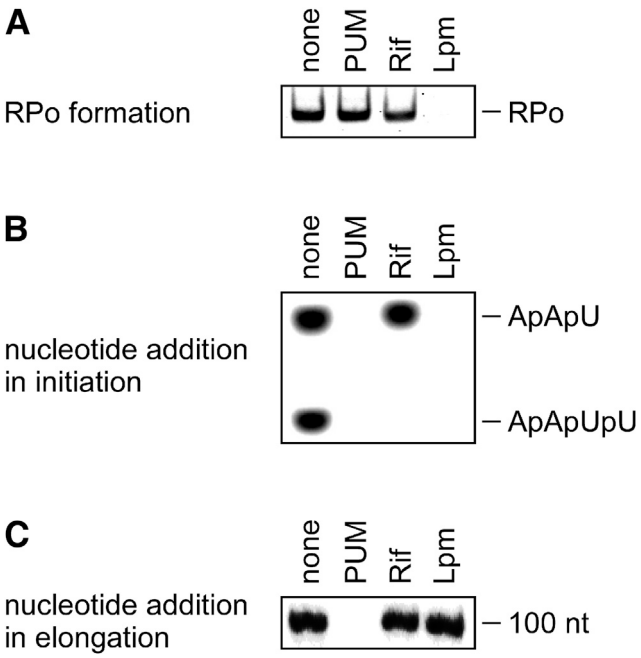

Figure S4. Mechanism of PUM: Inhibition of Nucleotide Addition, Related to Figure 3

(A) Absence of inhibition by PUM of formation of catalytically-competent RNAP-promoter open complex, RPo (*E. coli* RNAP).

(B) Inhibition by PUM of nucleotide addition in transcription initiation (*E. coli* RNAP).

(C) Inhibition by PUM of nucleotide addition in transcription elongation (*E. coli* RNAP).

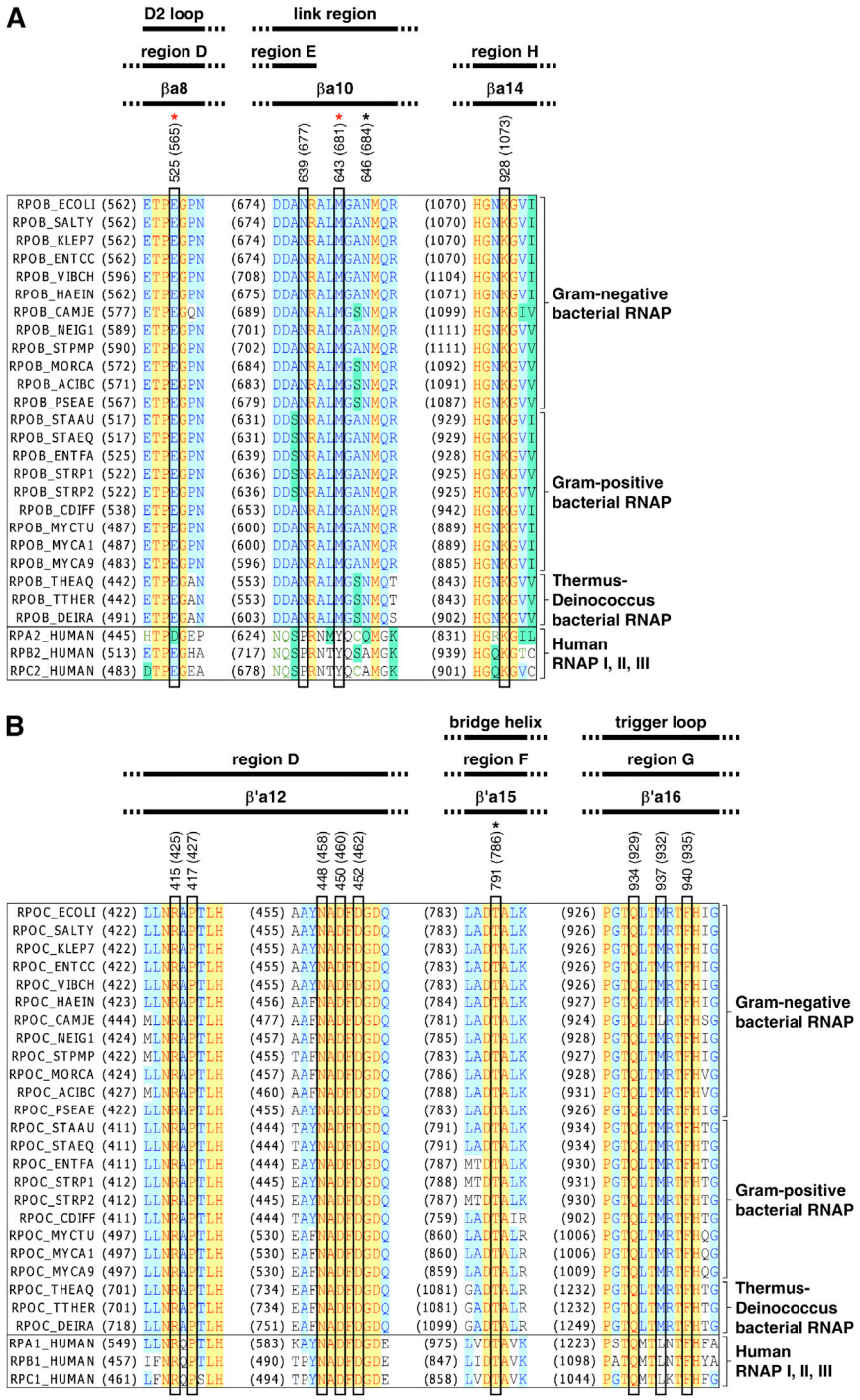

Figure S5. Interactions between RNAP and PUM: Sequence Alignments, Related to Figure 4

(A and B) Locations of residues that contact PUM in the sequences of RNAP β subunit (A) and RNAP β′ subunit (B). Sequence alignments for β and β′ subunits of bacterial RNAP (top 24 sequences in each panel) and corresponding subunits of human RNAP I, RNAP II, and RNAP III (bottom three sequences in each panel), showing locations of RNAP residues that contact PUM (black rectangles; numbered as in *S. pyogenes* and, in parentheses, as in *E. coli*; identities from Figure 4A), locations of residues at which substitutions conferring PUM-resistance are obtained in both *S. pyogenes* and *E. coli* (red asterisks; identities from Figures 2B, S3A, and S3B), locations of residues at which substitutions conferring PUM-resistance are obtained in *S. pyogenes* but not *E. coli* (black asterisks; identities from Figures 2B, S3A, and S3B), locations of RNAP structural elements (Weinzierl, 2010; Hein and Landick, 2010; top row of black bars), and RNAP conserved regions (Sweetser et al., 1987; Jokerst et al., 1989; Lane and Darst, 2010; next two rows of black bars). Species are as follows: *E. coli* (ECOLI), *Salmonella typhimurium* (SALTY), *Klebsiella pneumoniae* (KLEP7), *Enterococcus cloacae* (ENTCC), *Vibrio cholerae* (VIBCH), *Haemophilus influenzae* (HAEIN), *Campylobacter jejuni*

(legend continued on next page)

(CAMJE), *Neisseria gonorrhoeae* (NEIG1), *Stenotrophomonas maltophilia* (STPMP), *Moraxella catarrhalis* (MORCA), *Acinetobacter baumannii* (ACIBC), *Pseudomonas aeruginosa* (PSEAE), *Staphylococcus aureus* (STAAU), *Staphylococcus epidermidis* (STAEQ), *Enterococcus faecalis* (ENTFA), *Streptococcus pyogenes* (STRP1), *Streptococcus pneumoniae* (STRP2), *Clostridium difficile* (CDIFF), *Mycobacterium tuberculosis* (MYCTU), *Mycobacterium avium* (MYCA1), *Mycobacterium abscessus* (MYCA9), *Thermus aquaticus* (THEAQ), *Thermus thermophilus* (THETH), *Deinococcus radiodurans* (DEIRA), and *Homo sapiens* (HUMAN).